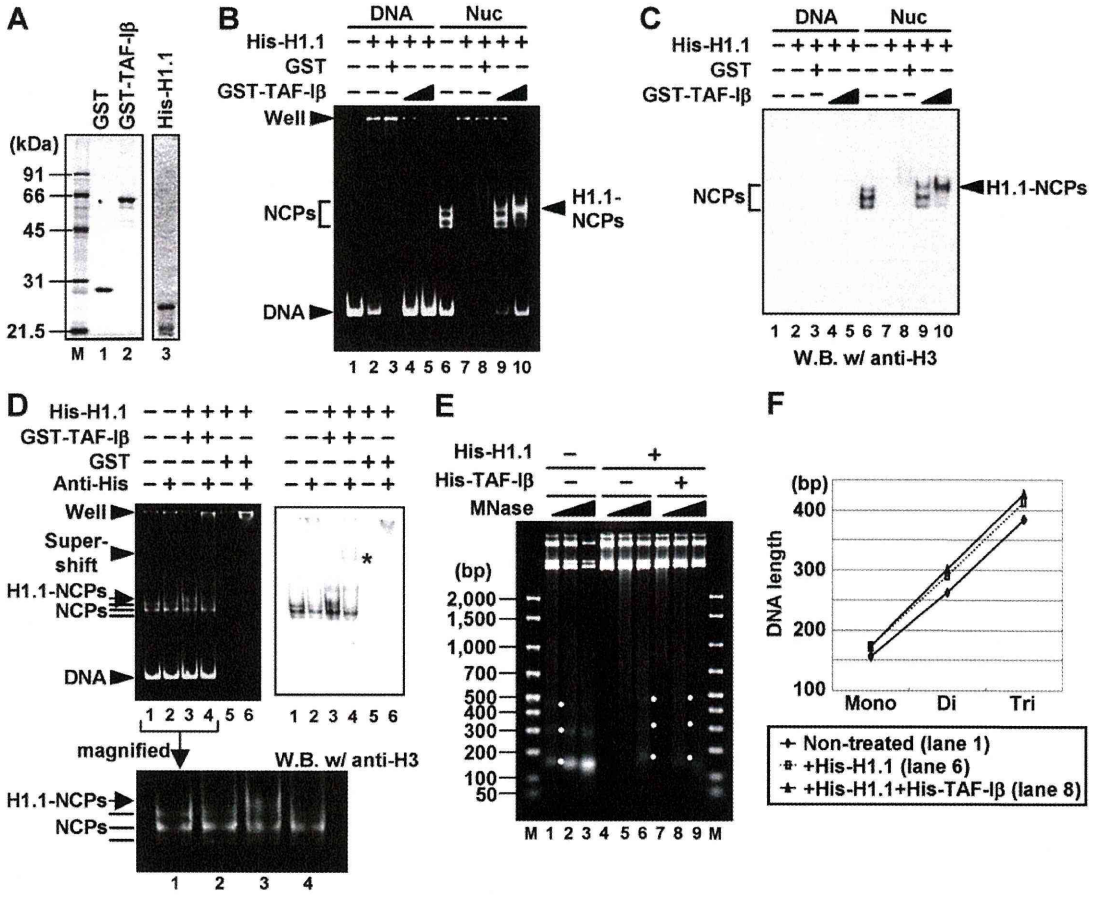

Fig. 2. In vitro linker histone chaperone activity of TAF-I. (**A**) Purified recombinant proteins. Recombinant GST, GST–TAF-Iβ, His–H1.1 proteins were separated by 10% SDS-PAGE and visualized with Coomassie Brilliant Blue staining. Lane M contains molecular size markers. (**B**) Formation of histone H1.1-NCPs complexes was examined by nucleoprotein gel analyses. The 196 bp *5S rRNA* gene fragments or NCPs (0.4 pmol of DNA) assembled on the same DNA with core histones were incubated without (lanes 1 and 6) or with His–H1.1 (0.6 pmol, lanes 2–5 and 7–10) pre-incubated without (lanes 2 and 7), with GST (30 pmol, lanes 3 and 8) or GST–TAF-Iβ dimer (1.7 pmol, lanes 4 and 9; 6.8 pmol, lanes 5 and 10). The complexes were separated by 6% non-denaturing PAGE, and DNA was visualized by GelRed staining. Positions of gel well, naked DNA and H1.1-NCPs are indicated by arrowheads. (**C**) Confirmation of histone H3 inclusion in NCPs and shifted complexes. After GelRed staining (shown in B), the gel piece was cut out, and proteins were blotted to membrane and subjected to western blotting using anti-histone H3 antibody. (**D**) Formation of histone H1.1–NCPs complexes was examined by super-shift assay. NCPs (0.4 pmol of DNA) were incubated without (lanes 1 and 2) or with His–H1.1 (0.6 pmol, lanes 3–6) pre-incubated with GST-TAF-Iβ (2 pmol dimer, lanes 3 and 4) or GST (9 pmol, lanes 5 and 6). The complexes were further incubated without (lanes 1, 3 and 5) or with anti-His antibody (lanes 2, 4 and 6), DNA was separated by 6% non-denaturing PAGE and visualized by GelRed staining (left panel). A magnified image of NCPs and H1.1-NCPs (lanes 1–4) is also shown. After GelRed staining, NCPs and H1.1-NCPs complexes were cut out from the gel, and proteins were blotted to membrane and subjected to western blotting using anti-histone H3 antibody (right panel). Positions of well, free DNA, NCPs, NCPs-H1.1 complexes and antibody-bound complexes are indicated. Asterisk also indicates super-shifted band. (**E**) Chromatosome formation was examined by MNase assays. The chromatin assembled on the plasmid pUC119-ML2 (200 ng of DNA) was incubated without (lanes 1–3) or with His–H1.1 (60 ng, lanes 4–9) pre-incubated without (lanes 4–6) or with His–TAF-Iβ (800 ng, lanes 7–9). Then, 5 mM $CaCl_2$ was added to samples followed by digestion with MNase (0.004 U/μl, lanes 1,4,7; 0.02 U/μl, lanes 2,5,8; 0.1 U/μl, lanes 3,6,9) at 37°C for 5 minutes. After stopping the reaction, DNA was purified and subjected to 1.5% agarose gel electrophoresis in 1 × TBE, and visualized by staining with GelRed. Lane M contains DNA size markers, and DNA sizes are indicated. (**F**) Graphical representation of MNase assays. DNA length of each nucleosomal ladder (shown by bullets in E) is plotted.

incubation with or without TAF-I or NAPs (molar ratio of chaperones to His–H1.1 were 6:1 or 24:1) (Fig. 3B). When His–H1.1 and naked DNA were incubated under non-saturated conditions (molar ratio of His–H1.1 to DNA was 0.5:1) without linker histone chaperones, a small fraction of aggregate was formed (which hardly entered the polyacrylamide gel) (Fig. 3B, lane 2). By contrast, when TAF-Iβ, NAP-1 and NAP-2 were added, this aggregate was dissociated. We also found that the ability of TAF-Iα to dissociate this aggregate was significantly lower than that of other chaperone proteins (Fig. 3B, lanes 3–6). Chromatosome samples pre-assembled without chaperones contained a low level of NCPs, chromatosomes and aggregates between naked DNA and His–H1.1 (Fig. 3B, lane 8). Upon addition of TAF-Iβ, chromatosome formation increased and the DNA–His–H1.1 aggregates dissociated in a dose-dependent manner (Fig. 3B, lanes 11–12). These results suggest that TAF-Iβ can dissociate a minor population of His–H1.1–DNA aggregates and transfer His–H1.1 to NCPs to form

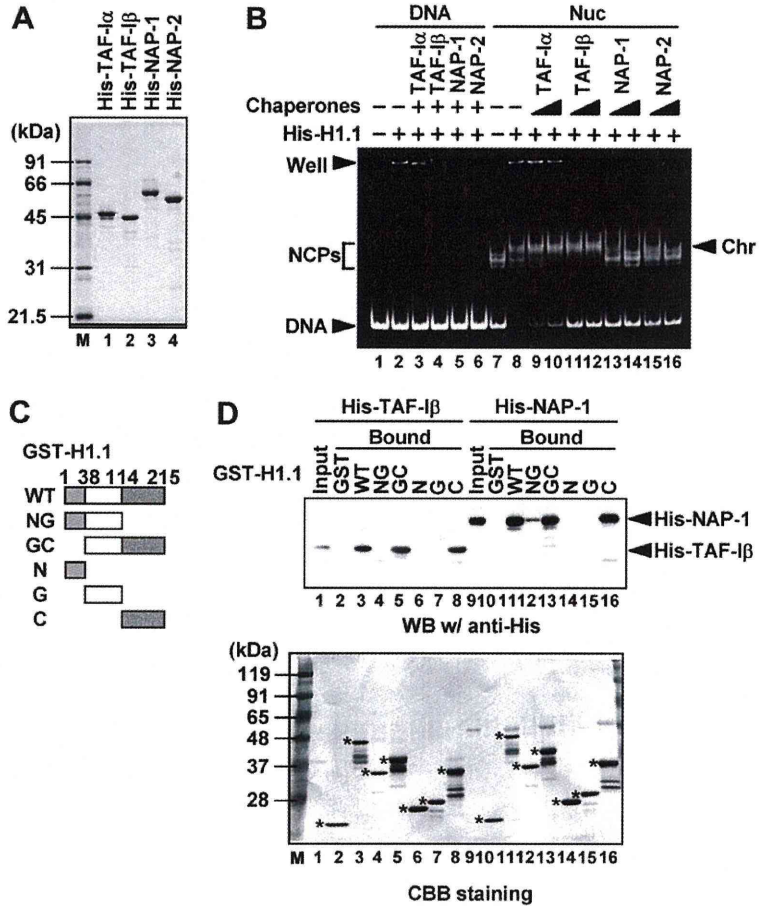

Fig. 3. TAF-I and NAPs have opposite linker histone chaperone activities in vitro. (**A**) Recombinant proteins. Recombinant His-tagged TAF-Iα, TAF-Iβ, NAP-1 and NAP-2 proteins (500 ng of each) were purified by affinity chromatography and were separated by 10% SDS-PAGE and visualized with Coomassie Brilliant Blue staining. Lane M contains molecular size markers. (**B**) Comparison of the biochemical properties of TAF-I with those of NAPs. Chromatosome was pre-assembled by incubation of NCPs (0.4 pmol of DNA) with histone H1.1 (0.2 pmol), followed by incubation with or without TAF-I or NAPs (1.2 and 4.8 pmol of dimer). Positions of well, free DNA, NCPs and chromatosome (Chr) are indicated by arrowheads. (**C**) Schematic representation of GST-tagged histone H1.1 wild type (WT) and deletion mutant proteins. N, G and C indicate N-terminal, globular and C-terminal domains, respectively. (**D**) GST pull-down assays. Interaction of His–TAF-Iβ and His–NAP-1 with GST or GST-H1.1 derivatives was examined by pull-down assays and western blotting using anti-His antibody (top panel). The 10% of His–TAF-Iβ or His–NAP-1 were loaded as Input. The same membrane was stained with Coomassie Brilliant Blue (lower panel). GST and GST-H1.1 derivatives are indicated by asterisks. Lane M contains molecular size markers.

chromatosomes. TAF-Iα also showed a similar activity, but its activity was lower than that of TAF-Iβ (Fig. 3B, compare lanes 9–10 and lanes 11–12). By contrast, NAP-1 and NAP-2 can dissociate not only DNA–His–H1.1 aggregates, but also chromatosome structure (Fig. 3B, compare lanes 8 and 13–16). We obtained similar results when the same experiments were performed in the presence of lower amounts of chaperones (supplementary material Fig. S2). Our results were in good agreement with the previous report (Saeki et al., 2005) that an excess amount of free NAP-1 facilitates the dissociation of histone H1 from chromatin. These in vitro studies indicate that both TAF-I and NAP proteins suppress and/or dissociate the non-specific aggregation formed by naked DNA and histone H1.1, and that TAF-I preferentially enhances chromatosome assembly, whereas NAP proteins enhance chromatosome disassembly.

We next examined which domain of histone H1.1 was required for the association with TAF-I and NAP-1. The structure of histone H1 is divided into N-terminal (N), globular (G) and C-terminal (C) domains (Raghuram et al., 2009). We prepared a series of six GST-tagged H1.1 deletion proteins (Fig. 3C), and the interaction between histone H1.1 domains and TAF-Iβ was assayed by GST pull-down (Fig. 3D). His-tagged TAF-Iβ could be precipitated with GST-H1.1 wild type (WT) but not with GST (Fig. 3D, lanes 2–3). When other H1.1 variants were used, both GST-H1.1 GC and C derivatives were precipitated with TAF-Iβ (Fig. 3D, lanes 5 and 8). Similar results were obtained using His–NAP-1 (Fig. 3D, lanes 9–16). These results indicate that both TAF-Iβ and NAP-1 bind to the highly basic C-terminal domain (CTD) of histone H1.1.

TAF-I affects the exchange kinetics of histone H1.1 in living HeLa cells

To investigate whether TAF-I and NAP-1 are involved in the exchange of histone H1 in living cells, we performed FRAP analyses using HeLa cells stably expressing H1.1–EGFP (Fig. 4A). When the cells were treated with siRNA to knock down TAF-I, the expression levels of TAF-Iα and TAF-Iβ were reduced to <10% of normal levels (Fig. 4B). Indirect immunofluorescence analyses showed that TAF-I is depleted in >90% of cells (Fig. 4C). When the cells were treated with NAP-1-specific siRNA, the expression level of NAP-1 was reduced to <25% of the normal level (Fig. 4B). We found that the recovery kinetics of H1.1–EGFP decreased in cells treated with TAF-I-specific siRNA, but not NAP-1-specific siRNA (Fig. 4D), suggesting that TAF-I, but not NAP-1, is involved in histone H1 dynamics as a histone chaperones in vivo.

In the above experiment, the expression level of H1.1–EGFP was approximately fivefold higher than that of endogenous total histone H1 (supplementary material Fig. S1C). To examine whether TAF-I-mediated alteration of H1.1–EGFP dynamics depends on the expression level of H1.1–EGFP, we further performed FRAP analyses using another cell line (clone #10)

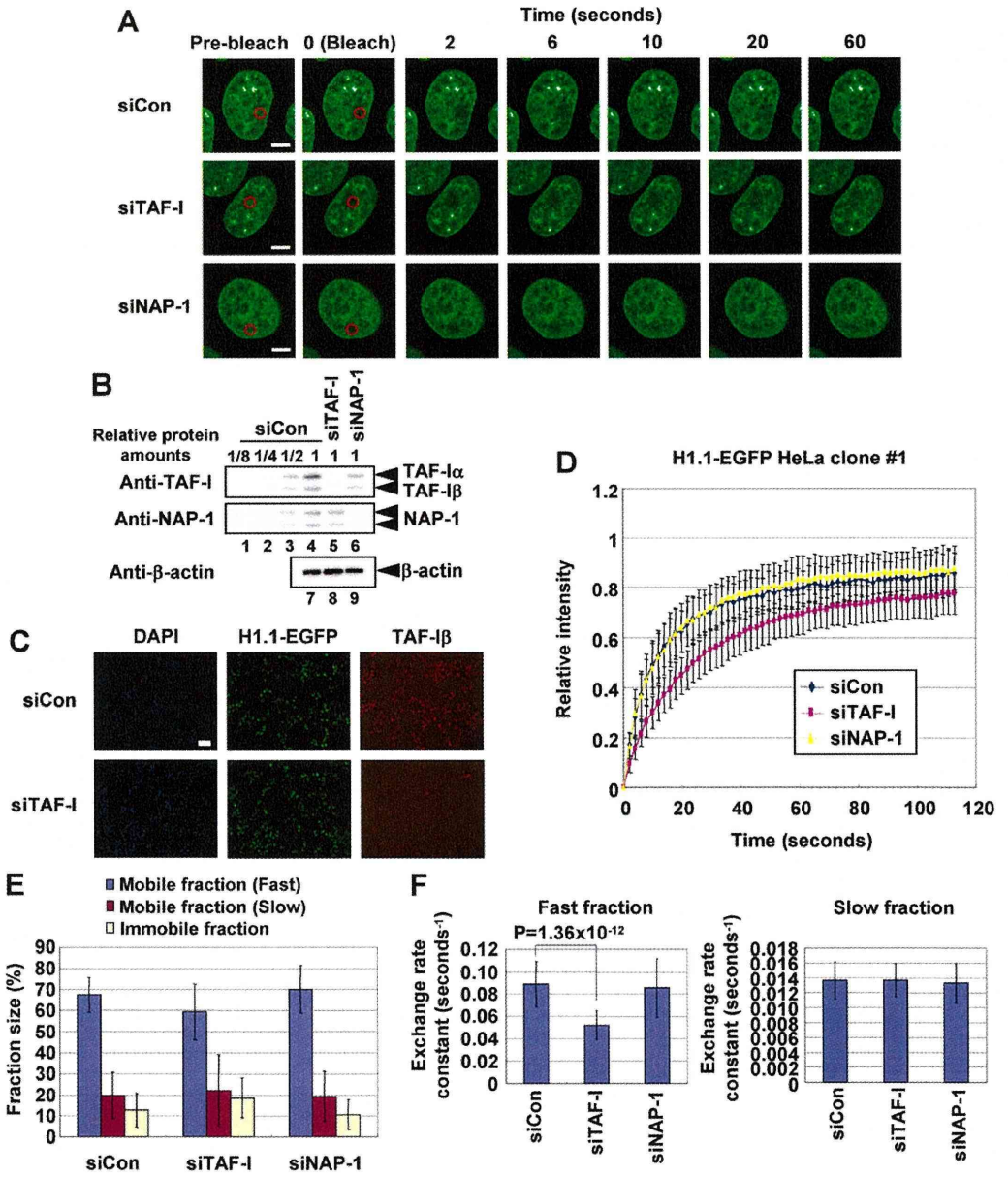

Fig. 4. Involvement of TAF-I in histone H1 dynamics in vivo. (**A**) FRAP images of H1.1–EGFP at indicated time points. Red circles indicate bleached regions. Scale bar: 5 μm. (**B**) Knockdown efficiency of TAF-I and NAP-1 was confirmed by western blotting using indicated antibodies. siCon represents control siRNA. β-actin serves as a loading control. (**C**) Populations of TAF-Iβ KD cells were examined by immunofluorescence analyses using anti-TAF-Iβ antibody. DNA was stained with DAPI. (**D**) FRAP recovery curve. Cells treated with control siRNA and siRNA to knock down TAF-I and NAP-1 were subjected to FRAP analyses. The means of the relative fluorescent intensity in the bleached area are indicated. Each data set consists of at least ten cells per experiment. Three independent experiments were performed for each cell. Error bars show s.d. (**E**,**F**) Graphical representation of fraction sizes and exchange rate constants. Exponential recovery curve fitting was performed and calculated fraction sizes (E) and exchange rate constants (F) are shown. Error bars represent s.d.

whose expression of H1.1–EGFP is <10% of that of clone #1 (supplementary material Fig. S3A). We found that the H1.1–EGFP dynamics also decreased in clone #10 cells treated with TAF-I-specific siRNA (supplementary material Fig. S3B–E). The expression level of endogenous histone H1 or H1.1–EGFP was unaffected by depletion of all chaperones (supplementary material Fig. S4A). The cell cycle profiles of cells treated with these siRNAs were not altered compared with control cells (supplementary material Fig. S4B,C). Therefore, we conclude that the alteration of H1.1–EGFP dynamics caused by TAF-I depletion is independent of the expression levels of histone H1 and the cell cycle.

Previously, it has been proposed that at least three distinct kinetic pools of chromatin-bound histone H1 exist: a weakly chromatin-bound pool, a strongly chromatin-bound pool and possibly, a stably bound (immobile) pool (Phair et al., 2004; Raghuram et al., 2009).

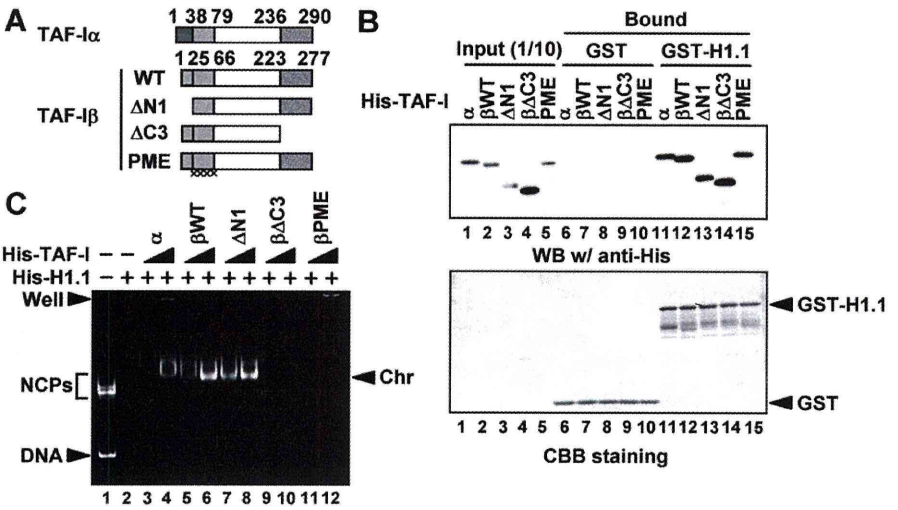

Fig. 5. Functional domains of TAF-I required for linker histone chaperone activity. (**A**) Schematic representation of TAF-I proteins. The N-terminal region specific for TAF-Iα (aa 1–38), that of TAF-Iβ (aa 1–25), coiled-coil region required for dimerization (aa 25–66) and C-terminal acidic region (aa 223–277) are indicated. Four point mutations in its hydrophobic surface of the coiled-coil region of TAF-IβPME are indicated by crosses. (**B**) GST pull-down assays. His–TAF-I derivatives pulled down with GST or GST–H1.1 were examined by western blotting using anti-His antibody (top panel). 10% of His–TAF-I derivatives were loaded as Input. To detect GST or GST–H1.1, the membrane used for western blotting was stained with Coomassie Brilliant Blue (bottom panel). (**C**) Chromatosome assembly assays. NCPs (0.4 pmol of DNA) were incubated without (lane 1) or with His–H1.1 (0.6 pmol, lanes 2–12) pre-incubated without (lanes 1–2) or with His–TAF-Iα, His–TAF-Iβ, His–TAF-IΔN1, His–TAF-IβΔC3 dimers (0.6 pmol, lanes 3,5,7,9; 2.4 pmol, lanes 4,6,8,10), and His–TAF-IβPME monomer (1.2 pmol, lane 11; 4.8 pmol, lane 12). The positions of gel well, naked DNA, NCPs and chromatosome (Chr) are indicated.

To clarify which pool of histone H1 was affected by TAF-I knockdown, we applied the double exponential recovery equation for curve fitting to distinguish the three pools (Sprague et al., 2004). We designated two mobile H1 populations as 'fast' and 'slow' fractions judged by their rate constants. The size of fast and slow fractions was not significantly different between cells treated with siRNA to knock down TAF-I and NAP-1 or control siRNA (Fig. 4E). However, the exchange rate constant of the fast fraction decreased in TAF-I-knockdown, but not in NAP-1-knockdown cells (Fig. 4F). We also showed that the dynamics of H1.1–EGFP in cells transfected with NASP-specific siRNA was poorly affected (supplementary material Fig. S5A–D). These results suggest that TAF-I, but neither NAP-1 nor NASP, is involved in the dynamic exchange of histone H1.1 in a weakly chromatin-bound H1 fraction in the mammalian somatic cell nucleus.

The acidic region of TAF-Iβ is essential for its linker histone chaperone activity, but not for H1 binding

To gain more insight into the linker histone chaperone activity of TAF-I, we prepared its mutant derivatives (Fig. 5A) and examined their in vitro H1 binding and the H1 chaperone activities by GST pull-down assays and nucleoprotein gel analyses. The adenoviral chromatin remodeling activity (Miyaji-Yamaguchi et al., 1999) and histone H1 binding activity of TAF-Iβ are higher than those of TAF-Iα (Fig. 1). In GST pull-down assays, both TAF-Iα and TAF-Iβ were bound to GST-H1.1 equally (Fig. 5B, lanes 11 and 12). TAF-IΔN1 lacking the N-terminal portions also bound to GST-H1.1 similarly to wild-type TAF-I (Fig. 5B, compare lanes 11–13), suggesting that the N-terminal regions, which differ between TAF-Iα and TAF-Iβ, are not required for H1 binding.

We next examined the chromatosome assembly activity of TAF-Iα, TAF-Iβ and TAF-IΔN1 using nucleoprotein gel analysis. DNA or NCPs were incubated with histone H1.1 pre-incubated with or without TAF-I derivatives. DNA or NCP and histone H1.1 aggregates were formed in the absence of the TAF-I proteins (molar ratio of His–H1.1 to DNA was 1.5:1) (Fig. 5C, lane 2). The addition of TAF-Iβ WT enhanced chromatosome formation in a dose-dependent manner (Fig. 5C, lanes 5 and 6). TAF-Iα WT also facilitated the chromatosome formation, whereas its activity was less than that of TAF-Iβ (Fig. 5C, compare lanes 3 and 4 with 5 and 6). TAF-IΔN1 facilitated the chromatosome formation as efficiently as TAF-Iβ WT (Fig. 5C, lanes 5 and 6 with 7 and 8). These results suggest that the N-terminal regions are not essential for chromatosome assembly. In addition, the N-terminal region of TAF-Iα hinders its chromatosome assembly activity.

We next examined the role of the C-terminal acidic region and the dimerization ability of TAF-Iβ in the linker histone chaperone activity. We have previously reported that the acidic region and the dimerization ability of TAF-Iβ are important for its core histone chaperone activity in vitro (Kato et al., 2007). TAF-IβΔC3 lacks the C-terminal acidic amino acid region, whereas TAF-IβPME has four point mutations in its hydrophobic surface of the coiled-coil region required for the dimerization ability (Miyaji-Yamaguchi et al., 1999). GST pull-down assays showed that both TAF-IβΔC3 and PME mutants bound to GST–H1.1 as efficiently as the wild type (Fig. 5B, compare lane 12 with lanes 14,15). By sharp contrast, neither TAF-IβΔC3 nor TAF-IβPME was found to have chromatosome assembly activity (Fig. 5C, lanes 9–12), indicating that the acidic region and its proper conformational orientation by dimer formation are essential for the linker histone chaperone activity of TAF-Iβ.

TAF-Iβ enhances the histone H1 fluidity depending on its acidic region

To examine whether an increase in the amount of TAF-I enhances histone H1 dynamics, we overexpressed TAF-I and

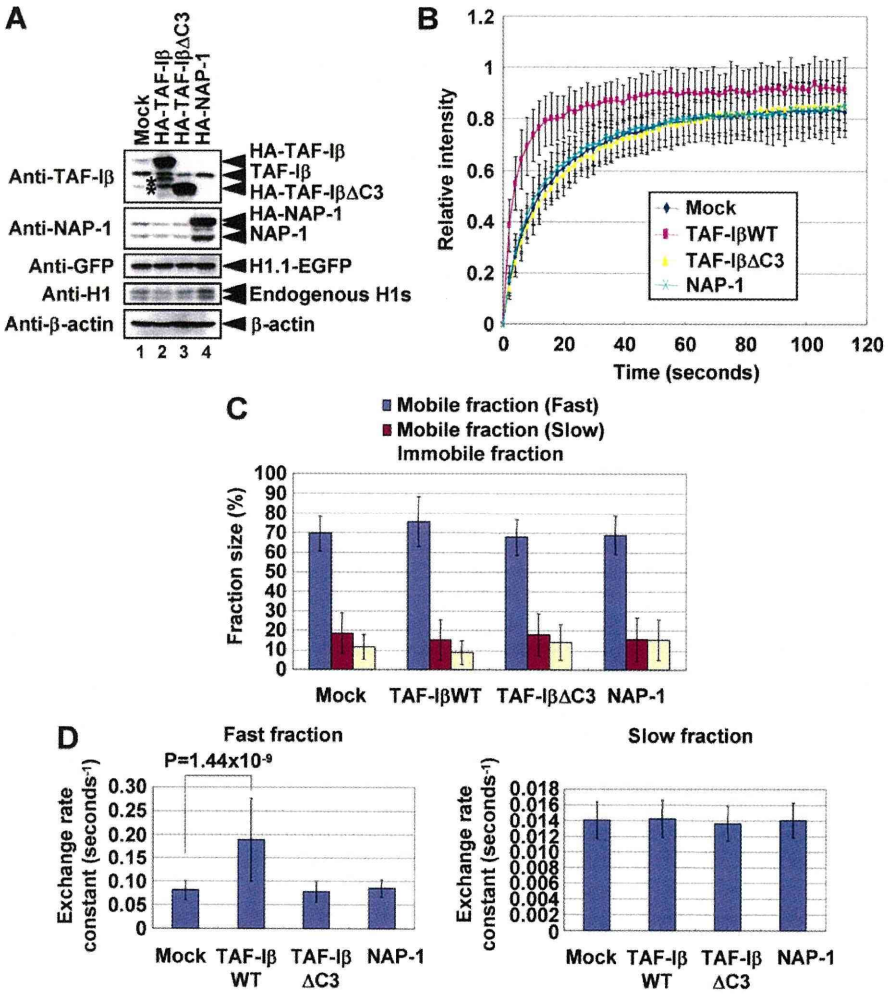

Fig. 6. Exogenously expressed TAF-Iβ enhances the histone H1 dynamics in its acidic region-dependent manner. (**A**) The expression level of exogenously expressed proteins. The extract prepared from cells transfected with plasmid DNAs encoding HA-tagged chaperones was separated by 10% SDS-PAGE, proteins were subjected to western blotting using indicated antibodies. Mock means control plasmid. β-actin serves as a loading control. Asterisks indicate predicted degradation products of HA–TAF-Iβ. (**B**) FRAP recovery curve. Cells transfected with plasmids DNA encoding HA-tagged chaperones and control plasmid were subjected to FRAP analyses. Each data set consists of at least ten cells per experiment. Three independent experiments were performed for each cell. Error bars show s.d. (**C**,**D**) Graphical representation of fraction sizes and exchange rate constants. Exponential recovery curve fitting was performed and calculated fraction sizes (C) and exchange rate constants (D) are shown. Error bars represent s.d.

measured the exchange kinetics of H1.1–EGFP in living cells. FRAP analyses were performed using the H1.1–EGFP cell line overexpressing hemagglutinin (HA)-tagged TAF-Iβ, the linker histone chaperone activity-deficient TAF-IβΔC3 mutant (Fig. 5B) and NAP-1. Cells were transfected with plasmids expressing HA–TAF-Iβ, HA–TAF-IβΔC3 and HA–NAP-1. HA–TAF-Iβ, HA–TAF-IβΔC3 or HA–NAP-1 was expressed in approximately 80% of cells (supplementary material Fig. S6), and the each expression level was approximately 25 times higher than their respective endogenous levels (Fig. 6A). The dynamics of H1.1–EGFP was robustly enhanced in cells overexpressing HA–TAF-Iβ, whereas both HA–TAF-IβΔC3 and HA–NAP-1 affected the recovery kinetics only slightly (Fig. 6B). The exchange rate constant of the fast fraction in cells expressing HA–TAF-Iβ was increased compared with that in mock-transfected cells, whereas there was no significant difference in the each fraction size and the exchange rate constant of the slow fraction (Fig. 6C,D). We also observed that the exchange rate constant of the fast fraction was slightly enhanced by HA–sNASP expression, although this effect was less significant ($P = 2.50 \times 10^{-2}$) (supplementary material Figs S7A–D and S8). It is possible that HA–sNASP affects the dynamics of H1.1–EGFP indirectly because it was not efficiently co-precipitated with H1.1–FLAG compared with TAF-I (supplementary material Fig. S7E). Neither HA–TAF-IβΔC3 nor HA–NAP-1 showed significant change in the exchange rate constant.

FRAP analyses suggested that TAF-Iβ enhances the dissociation of H1.1 from chromatin in vivo. To address this further, we examined the association level of H1.1–EGFP with chromatin under several biochemical extraction conditions in combination with overexpression of TAF-Iβ (Fig. 7A–C). The expression level of both H1.1–EGFP and histone H3 was little affected by the overexpression of HA–TAF-Iβ and HA–TAF-IβΔC3 (Fig. 7A). The expression levels of HA–TAF-Iβ and HA–TAF-IβΔC3 were approximately 25 times higher than that of endogenous TAF-Iβ (Fig. 7B). In mock-transfected cells, small amount of H1.1–EGFP or histone H3 was recovered in a supernatant (sup) fraction (Fig. 7C, both are approximately <10% of those in pellet fractions). Significant amount of H1.1–EGFP (approximately 30% of pellet) was recovered in the sup fraction of cells when HA–TAF-Iβ was overexpressed, independently of $MgCl_2$ concentrations, which influence chromatin compaction (Arya and Schlick, 2009) (Fig. 7C). By contrast, the amount of histone H3 in the sup fraction was significantly less than that of H1.1–EGFP even when TAF-Iβ was overexpressed. These results suggest that overexpression of TAF-Iβ enhances the dissociation

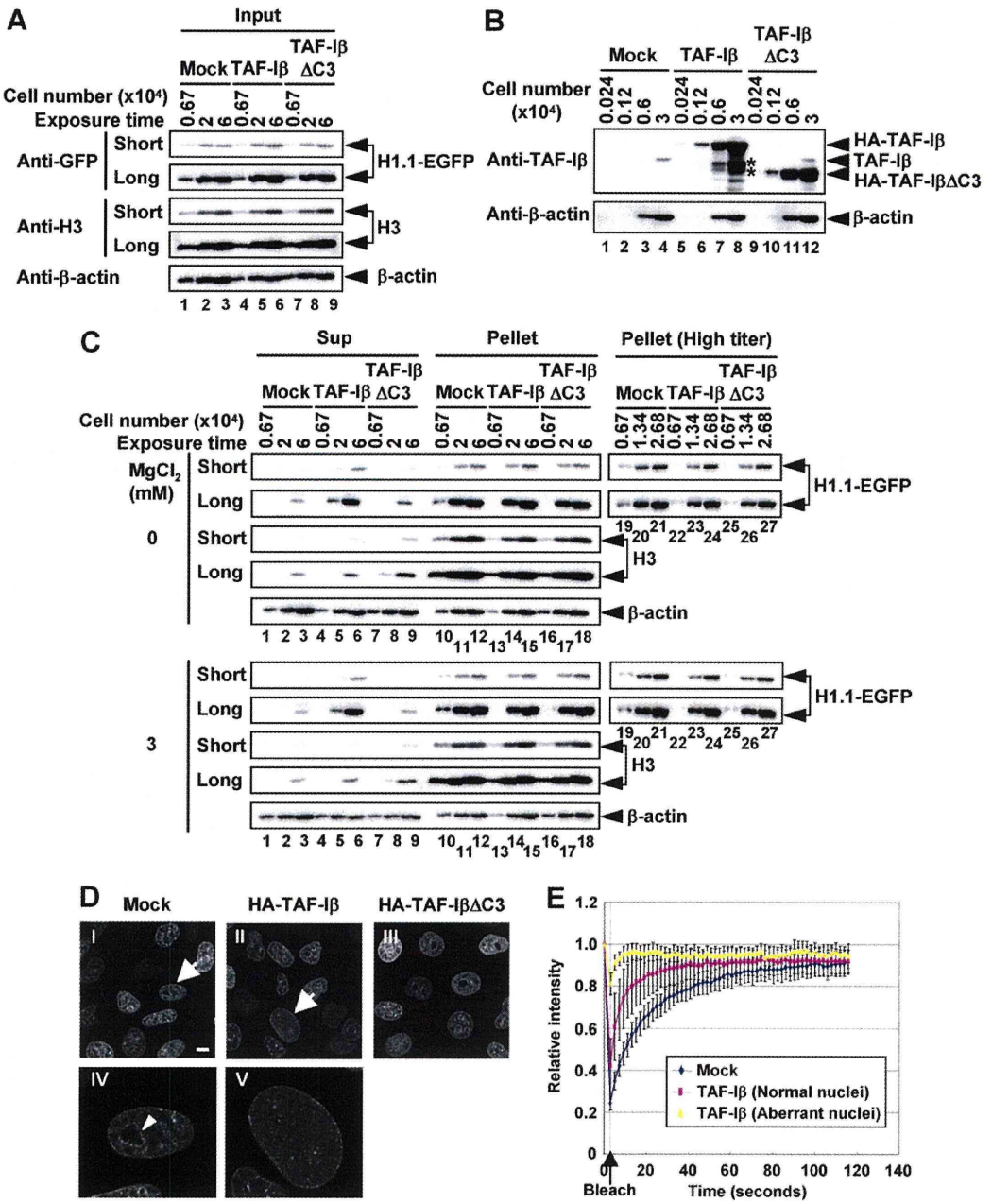

Fig. 7. TAF-I facilitates the dissociation of histone H1 from native cellular chromatin. (**A**) The expression levels of histone H1.1–EGFP and histone H3 were examined by western blotting analyses using indicated antibodies. Loaded cell numbers are shown above figure. Two images taken by different exposure durations (short and long) are shown. (**B**) The expression levels of endogenous TAF-Iβ, exogenous HA–TAF-Iβ and HA–TAF-IβΔC3 were examined by western blotting analyses using indicated antibodies. (**C**) Subcellular fractionation was carried with cells expressing exogenous TAF-Iβ and TAF-IβΔC3. The amounts of histones H1.1–EGFP and H3 in supernatant and pellet fractions were examined. β-actin serves as a loading control. Loaded cell numbers were shown above panels. Two photos taken by different exposure durations (short and long) are shown. Additional western blotting analyses were performed using high titer-GFP antibody and smaller cell numbers for pellet samples (lanes 19–27). (**D**) TAF-Iβ overexpression induces nuclear morphological changes. Images of HeLa cells stably expressing H1.1–EGFP transfected with plasmid DNA encoding HA–TAF-Iβ (II) or HA–TAF-IβΔC3 (III) and control plasmid (I) are shown. Scale bar: 10 μm. IV and V are magnified images of indicated nuclei by arrows in images I and II, respectively. The nucleolar peripheral heterochromatin region is also indicated by arrowhead in image IV. (**E**) H1.1–EGFP dynamics was significantly enhanced in morphologically aberrant nuclei generated by TAF-Iβ overexpression. FRAP was performed in mock-transfected cells, and cells overexpressing TAF-Iβ including morphologically normal and aberrant nuclei (V as shown in D). Relative fluorescent intensities (measure before bleaching is set to 1) were plotted. The time point of bleaching is indicated by arrow. Each data set consists of at least ten cells per experiment. Three independent experiments were performed for each cell. Error bars represent s.d.

of histone H1 but not histone H3 from chromatin. This notion is in good agreement with the result obtained from FRAP analyses. We found that the cell population with aberrant nuclear morphology was increased by overexpression of TAF-Iβ. Nuclei with aberrant morphology in cells overexpressing TAF-Iβ became relatively enlarged compared with that of normal cells (Fig. 7D and supplementary material Fig. S9A). Furthermore, the localization of H1.1–EGFP became homogenous, and higher-ordered nuclear structures such as the nucleolus were invisible in those nuclei (Fig. 7D). Approximately 25% of total cells overexpressing TAF-Iβ showed morphologically aberrant nuclei (supplementary material Fig. S9B). In morphologically aberrant nuclei, the H1.1–EGFP mobility was extremely rapid, suggesting that H1.1–EGFP is greatly diffused (Fig. 7E). The cell cycle profiles of cells expressing HA–TAF-Iβ, HA–TAF-IβΔC3 and HA–NAP-1 were similar to that of mock-transfected cells (supplementary material Fig. S10A,B). However, we found that the DNA content becomes lower in approximately 20% of cells by overexpression of TAF-Iβ (supplementary material Fig. S10A,B). These cells would not be apoptotic because they were negative in Annexin-V staining (data not shown). It is possible that cells with aberrant nuclei are alive, but the chromatin (and/or nuclei themselves) in these cells becomes fragile. Collectively, these results suggest that TAF-Iβ enhances the dissociation of histone H1 and that its C-terminal acidic region is crucial for the histone H1 chaperone activity.

Discussion

Here, we have demonstrated that TAF-I functions as a linker histone chaperone, which is involved in the regulation of histone H1 exchange in the mammalian somatic cell nucleus. We observed that TAF-I is associated with histone H1 in the HeLa cell nuclear soluble fraction (Fig. 1A–D). More importantly, NAP-1 and NASP, previously reported linker histone chaperone candidates, are poorly associated with histone H1 in somatic cells (Fig. 1A,B). From immunoprecipitation and MS/MS analyses, we found that TAF-I associates with at least three cell-cycle-dependent variants and one cell-cycle-independent histone H1 variant (H1.2, H1.4, H1.5 and H1X) in the nuclear soluble fraction of HeLa cells (Fig. 1C,D, and supplementary material Tables S1 and S2). We found that TAF-I associates with histone H1.0 and H1.1 when exogenously expressed in HeLa cells (Fig. 1A,B), suggesting that TAF-I has intrinsic ability to bind histone H1.0 and H1.1 in vivo. Histone H1 variants have similar primary structures, but histone H1.0 and H1X are different from the five somatic histone H1 subtypes (H1.1–H1.5). Because TAF-I binds not only to three cell-cycle-dependent histone H1 subtypes, but also H1X, it is possible that overall structure, but not the primary structure of histone H1 CTD (in the case of H1.1 in Fig. 3D), is important for the interaction between TAF-I and histone H1. In contrast to the high homology of histone H1 variants, their expression levels differ among organs or cell types. It was suggested that the expression levels of histone H1.0 and H1.1 are relatively low compared with that of four somatic histone H1 subtypes (H1.2–H1.5) in HeLa cells, whereas the expression levels of histone H1.2, H1.3 and H1.4 have not been reported (Wisniewski et al., 2007). Therefore, it is possible that we were unable to detect histone H1.0 and H1.1 (as well as H1.3) by MS/MS analyses, whereas TAF-I was found to bind to a variety of histone H1 variants.

Both TAF-I and NAP-1 have modulatory activity in histone H1 binding to chromatin in vitro (Fig. 3B). However, it is not clear how these proteins function differently. TAF-Iβ and NAP-1 are folded into a similar structure, whereas their backbone helices are shaped differently, and NAP-1 has an extra inserted helix (Muto et al., 2007). Such structural differences between TAF-Iβ and NAP-1 might contribute to the difference in the modulation of histone H1 dynamics. It has been speculated that the chromatosome is formed through interaction between histone H1 and the C-terminal tail of histone H2A (Luger et al., 1997). Because NAP-1, but not TAF-I, has binding specificity for histone H2A, NAP-1 might modulate the binding between histone H1 and histone H2A through its interaction with histone H2A. Alternatively, this interaction could have a role in NAP-1-mediated dissociation of chromatosome structure. Although our observation suggests that NAP-1 binds poorly to histone H1 in mammalian somatic cells, we cannot exclude the possibility that NAP-1 is also involved in histone H1 metabolism in a cell-lineage-specific manner. In support of this view, it was reported that histone H1 dissociates from chromatin when NAP-1 is transiently relocalized in the nucleus in mouse primordial germ cells on embryonic day 11.5 (Hajkova et al., 2008), suggesting that NAP-1 removes histone H1 to alter the chromatin structure for epigenetic reprogramming of germ cell lines.

NASP preferentially associates with histone H3.2, rather than H1, in the nuclear soluble fraction (Fig. 1A). FRAP analyses also revealed that NASP is not significantly involved in the exchange of histone H1 (supplementary material Figs S4 and S6). Therefore, it is probable that a major fraction of NASP forms the multi-chaperone complex with Asf1, CAF-I and histone H3.1 (Tagami et al., 2004), although we cannot rule out the possibility that a small fraction of NASP is associated with histone H1.

Previous studies have shown that HMG proteins affect the in vivo dynamics of histone H1 through their competitive binding to the nucleosomal binding sites of histone H1 (Catez et al., 2004; Rochman et al., 2009). These studies suggest the possible involvement of competition among linker histone, regulatory protein and nucleosomal DNA in the linker histone dynamic equilibrium. We have shown that TAF-I is a novel *trans*-acting factor involved in histone H1 dynamics by its chaperone activity but not competitive binding to chromatin. FRAP analyses indicated that TAF-I affects the exchange kinetics of the fast mobile (thus, low affinity for chromatin) histone H1 population (Figs 4 and 6). Although the biological significance of the two kinetic fractions of histone H1 is still unclear, it is likely that the fast mobile histone H1 population represents a non-specific DNA-binding and/or locus-specific but unstable chromatosome structure. Previously, it was suggested that weak binding between histone H1 and chromatin occurs through the interaction between its CTD and DNA (Raghuram et al., 2009). Because TAF-I preferentially localizes in euchromatic regions, it is possible that TAF-I modulates the DNA-binding affinity of euchromatic (probably loosely chromatin-bound) histone H1 through its interaction with CTD, and thus is involved in a certain nuclear reaction(s) such as transcription.

TAF-I could not efficiently dissociate histone H1 from chromatin in vitro even when present in excess (Fig. 3B), whereas FRAP analyses strongly suggested the involvement of TAF-I in the histone H1 assembly and disassembly in vivo (Figs 4, 6 and 7). Currently, it is not clear what causes such functional differences. We speculate that phosphorylation of histone H1 is cooperatively involved in its dissociation by TAF-I in vivo, because CDK-dependent phosphorylation of histone H1 is

involved in the regulation of its dynamics (Yellajoshyula et al., 2006). Alternatively, TAF-Iβ forms a protein complex including ProTα in vivo (Karetsou et al., 2004). ProTα also has linker histone chaperone activity and is involved in the nuclear dynamics of histone H1 (George and Brown, 2010; Karetsou et al., 1998). Our in vitro analyses revealed that TAF-I and NAP-1 preferentially bind to the histone H1 CTD, whereas ProTα binds to its globular domain (Karetsou et al., 1998). Furthermore, ProTα preferentially mediates histone H1 dissociation from chromatin in vitro (Karetsou et al., 1998). It is therefore possible that a putative TAF-I–ProTα complex efficiently regulates the exchange of histone H1 on chromatin using their functional differences in vivo.

Histone-H1-dependent chromatin dynamics is important for a variety of biological phenomena, including early embryogenesis, cell differentiation and cell senescence (Funayama et al., 2006; Godde and Ura, 2009; Meshorer et al., 2006; Yellajoshyula and Brown, 2006). Our results indicate that TAF-I could modulate the higher-ordered chromatin structure (Fig. 7D,E). It could be worthwhile to examine whether TAF-I is involved in nuclear reprogramming by re-organizing the whole chromatin structure through its linker histone chaperone activity, and thus is widely involved in cell fates.

Materials and Methods

Cell culture, construction of cell lines and FACS analyses

Maintenance of HeLa cells expressing H2A–FLAG and H1.0–FLAG, and construction of HeLa cells expressing H3.2–FLAG, H1.1–FLAG, H1.2–FLAG and H1.1–EGFP, were followed as described (Okuwaki et al., 2010). Stably expressing cells were selected in growth medium containing 1 mg/ml G418, and single colonies were picked to generate clonal cell lines. FACS analyses were performed by following standard protocols.

Antibodies and indirect immunofluorescence analyses

Antibodies used in this study were as follows: anti-CAF-Ip150 (clone SS1) and anti-Asf1b antibodies gifts from Alain Verreault (University of Montreal, Canada); anti-NAP-1, anti-Spt16 and anti-histone H1 (clone AE4) antibodies from SantaCruz Biotech; anti-NASP antibody from ProteinTech Group; anti-histone H3 and anti-histone H1X antibodies from Abcam; anti-β-actin, anti-FLAG-tag and anti-His-tag antibodies from Sigma; anti-GFP antibody from Nacalai tesque; anti-HA-tag antibody (clone 3F10) from Roche; anti-TAF-Iβ antibody (monoclonal antibody KM1720; Kirin-Kyowa Hakko) (Nagata et al., 1998); anti-TAF-I polyclonal antibody, which was generated in rabbits using recombinant TAF-IβΔC3 as an antigen. For indirect immunofluorescence analyses, antibodies conjugated to Alexa Fluor 488 and Alexa Fluor 568 were from Invitrogen. Images were obtained using microscopes (LSM EXCITER or Axioplan2 imaging; Carl Zeiss Microimaging).

Immunoprecipitation, liquid chromatography and mass spectrometry analyses (LC-MS/MS)

Preparation of cytoplasmic and nuclear extracts from HeLa cells and immunoprecipitation were performed as described (Okuwaki et al., 2010). Samples for LC-MS/MS analyses were prepared by carving out immunoprecipitated proteins from silver-stained gel and in-gel trypsin digestion. Mass spectrometry data were obtained using LC-MS/MS apparatus (ZAPLOUS; AMR) and analyzed with MASCOT software.

Nucleosome reconstitution and chromatosome assembly-disassembly assay

Recombinant chaperone proteins were prepared as described previously (Matsumoto et al., 1999; Miyaji-Yamaguchi et al., 1999; Okuwaki et al., 2005). His-tagged H1.1, GST-tagged H1.1, and its mutant derivatives, were also expressed in *E. coli* BL21 (DE3). Core histones were purified from HeLaS3 cells. NCPs were assembled with 196 bp sea urchin *5S rRNA* gene fragment and core histones by the salt dilution method as described previously (Okuwaki et al., 2010). Chromatosome assembly-disassembly assays were performed essentially as follows: Briefly, naked 5S DNA or NCPs were incubated at 30°C for 30 minutes with His–H1.1 pre-incubated at 30°C for 30 minutes with or without histone chaperone proteins. Samples were then subjected to a 5% non-denaturing polyacrylamide gel electrophoresis in 0.5 × TBE buffer, and then DNA was visualized by staining with GelRed (Biotium). For western blotting, proteins and DNA on the gel were transferred to a PVDF membrane. For super-shift assays, samples were incubated with anti-His antibody at 30°C for 15 minutes just before loading on the polyacrylamide gel. For MNase assays, chromatin was assembled with plasmid pUC119-ML2 (Kato et al., 2007) and core histones by the salt dilution method. The reconstituted chromatin (200 ng DNA-equivalent) was incubated at 30°C for 30 minutes with or without His–H1.1 pre-incubated at 30°C for 30 minutes with or without His–TAF-Iβ. DNA was purified, subjected to 1.5% agarose gel electrophoresis in 1 × TBE buffer and visualized by staining with GelRe. DNA images were analyzed with LAS-4000UVmini image analyzer (Fuji Film).

siRNA and plasmid transfection

All Stealth siRNAs were obtained from Invitrogen. siRNAs were transfected with Lipofectamine2000 (Invitrogen). Cells were re-plated at 72 hours after transfection and then incubated for 12 hours. Cells were transfected with siRNAs once again and further incubated for 48 hours after the second transfection. Cells were transfected with plasmid DNAs expressing HA-tagged proteins using GeneJuice (Novagen) in combination with plasmid pBabe-puro expressing puromycin-resistant gene. At 24 hours after transfection, 2 μg/ml of puromycin dihydrochloride was directly added to the culture medium, and cells were further incubated for 24 hours to remove untransfected cells.

FRAP analyses

HeLa cells stably expressing H1.1–EGFP grown on 35-mm-diameter glass base dishes were transfected with Stealth siRNA or plasmid DNAs. The dish was set on an inverted microscope (LSM EXCITER; Carl Zeiss Microimaging, Inc.) in an air chamber at 37°C, and the mobility of EGFP-tagged histone H1.1 was analyzed by photobleaching with a Plan-Apochromat 63 × /1.4 oil objective. A 2 μm spot was bleached using 85% transmission of 488 nm Ar laser (50 iterations), and images were collected (512 × 512 pixels, zoom 1, scan speed 9, pinhole 1 airy unit, LP505 emission filter and 1% transmission of 488-nm Ar laser with 70% output power) every 2 seconds. The fluorescence intensity of the bleached area was measured. Subtracting the background, normalizing by fluorescent decay during scan and exponential recovery curve fitting were performed using FRAP for ZEN software (Carl Zeiss Microimaging). The double exponential recovery curve is described by the equation, $F(t)=A1(1-e^{-K1t})+A2(1-e^{-K2t})$ (Sprague et al., 2004). $F(t)$ indicates the normalized fluorescent intensity at each time point where the measurement just before bleaching is set to be 1 and that just after bleaching is set to be 0. A1 and A2 indicate the ratio of fast and slow mobile fraction each, and the ratio of total mobile fraction (A) is calculated by the equation, A=A1+A2. Conversely, the ratio of immobile fraction is calculated by a formula: 1–A. K1 and K2 indicate the rate constants for the fluorescent exchange between bleached and un-bleached regions. FRAP recovery curves were drawn in Excel2003 where the intensity was normalized to the initial intensity before bleaching.

Subcellular fractionation

The basis of fractionation methods was essentially as described (Capco et al., 1982). Cells transfected with plasmids and selected with puromycin were incubated in an extraction buffer (10 mM PIPES-NaOH, pH 6.8, 100 mM NaCl, 1 mM EGTA, 300 mM sucrose, 1 mM PMSF, 1 mM NaF, 10 mM β-D-glycerophosphate, 1 mM Na_3VO_4 and 0.1% NP40) with or without 3 mM $MgCl_2$ on ice for 10 minutes. Supernatant and pellet fractions were separated by centrifugation, and subjected to 15% SDS-PAGE followed by western blot analyses.

Acknowledgements

We thank Alain Verreault (University of Montreal, Canada) for anti-CAF-Ip150 and anti-Asf1b antibodies, Takashi Minowa, Ayumu Yosida (National Institute for Materials Science, Japan), and Masamitsu N. Asaka (University of Tsukuba, Japan) for kind support with LC-MS/MS analyses, Shinichi Tate (Hiroshima University, Japan) for human histone expression plasmids, Miharu Hisaoka (University of Tsukuba) for purification of HeLa core histones, Shoko Saito and Takafumi Yokokawa (University of Tsukuba) for kind support for FACS analyses and Kiong Ho (University of Tsukuba) for discussion and proofreading of this manuscript.

Funding

This work was supported by Grants-in-aid for Scientific Research from the Ministry of Education, Culture, Sports, Science and Technology of Japan (to M.O. and K.N.), in part by PRESTO from Japan Science and Technology Agency and Special Coordination Funds for Promoting Science and Technology (to M.O.).

Supplementary material available online at
http://jcs.biologists.org/lookup/suppl/doi:10.1242/jcs.083139/-/DC1

References

Ahmad, K. and Henikoff, S. (2002). The histone variant H3.3 marks active chromatin by replication-independent nucleosome assembly. *Mol. Cell* **9**, 1191-1200.

Alekseev, O. M., Bencic, D. C., Richardson, R. T., Widgren, E. E. and O'Rand, M. G. (2003). Overexpression of the Linker histone-binding protein tNASP affects progression through the cell cycle. *J. Biol. Chem.* **278**, 8846-8852.

Alekseev, O. M., Widgren, E. E., Richardson, R. T. and O'Rand, M. G. (2005). Association of NASP with HSP90 in Mouse Spermatogenic Cells. *J. Biol. Chem.* **280**, 2904-2911.

Arya, G. and Schlick, T. (2009). A tale of tails: how histone tails mediate chromatin compaction in different salt and linker histone environments. *J. Phys. Chem. A* **113**, 4045-4059.

Capco, D. G., Wan, K. M., and Penman, S. (1982). The Nuclear Matrix: Three-Dimensional Architecture and Protein Composition. *Cell* **29**, 847-858.

Catez, F., Yang, H., Tracey, K. J., Reeves, R., Misteli, T. and Bustin, M. (2004). Network of dynamic interactions between histone H1 and high-mobility-group proteins in chromatin. *Mol. Cell. Biol.* **24**, 4321-4328.

De Koning, L., Corpet, A., Haber, J. E. and Almouzni, G. (2007). Histone chaperones: an escort network regulating histone traffic. *Nat. Struct. Mol. Biol.* **14**, 997-1007.

Fan, Y., Nikitina, T., Morin-Kensicki, E. M., Zhao, J., Magnuson, T. R., Woodcock, C. L. and Skoultchi, A. I. (2003). H1 linker histones are essential for mouse development and affect nucleosome spacing in vivo. *Mol. Cell. Biol.* **23**, 4559-4572.

Funayama, R., Saito, M., Tanobe, H. and Ishikawa, F. (2006). Loss of linker histone H1 in cellular senescence. *J. Cell. Biol.* **175**, 869-880.

George, E. M. and Brown, D. T. (2010). Prothymosin alpha is a component of a linker histone chaperone. *FEBS Lett.* **584**, 2833-2836.

Godde, J. S. and Ura, K. (2009). Dynamic alterations of linker histone variants during development. *Int. J. Dev. Biol.* **53**, 215-224.

Hajkova, P., Ancelin, K., Waldmann, T., Lacoste, N., Lange, U. C., Cesari, F., Lee, C., Almouzni, G., Schneider, R. and Surani, M. A. (2008). Chromatin dynamics during epigenetic reprogramming in the mouse germ line. *Nature* **452**, 877-881.

Happel, N. and Doenecke, D. (2009). Histone H1 and its isoforms: contribution to chromatin structure and function. *Gene* **431**, 1-12.

Jullien, J., Astrand, C., Halley-Stott, R. P., Garrett, N. and Gurdon, J. B. (2010). Characterization of somatic cell nuclear reprogramming by oocytes in which a linker histone is required for pluripotency gene reactivation. *Proc. Natl. Acad. Sci. USA* **107**, 5483-5488.

Karetsou, Z., Martic, G., Tavoulari, S., Christoforidis, S., Wilm, M., Gruss, C. and Papamarcaki, T. (2004). Prothymosin alpha associates with the oncoprotein SET and is involved in chromatin decondensation. *FEBS Lett.* **577**, 496-500.

Karetsou, Z., Sandaltzopoulos, R., Frangou-Lazaridis, M., Lai, C. Y., Tsolas, O., Becker, P. B. and Papamarcaki, T. (1998). Prothymosin alpha modulates the interaction of histone H1 with chromatin. *Nucleic Acids Res.* **26**, 3111-3118.

Kato, K., Miyaji-Yamaguchi, M., Okuwaki, M. and Nagata, K. (2007). Histone acetylation-independent transcription stimulation by a histone chaperone. *Nucleic Acids Res.* **35**, 705-715.

Kawase, H., Okuwaki, M., Miyaji, M., Ohba, R., Handa, H., Ishimi, Y., Fujii-Nakata, T., Kikuchi, A. and Nagata, K. (1996). NAP-I is a functional homologue of TAF-I that is required for replication and transcription of the adenovirus genome in a chromatin-like structure. *Genes Cells* **1**, 1045-1056.

Kimura, H. and Cook, P. R. (2001). Kinetics of core histones in living human cells: little exchange of H3 and H4 and some rapid exchange of H2B. *J. Cell. Biol.* **153**, 1341-1353.

Lever, M. A., Th'ng, J. P., Sun, X. and Hendzel, M. J. (2000). Rapid exchange of histone H1.1 on chromatin in living human cells. *Nature* **408**, 873-876.

Luger, K., Mader, A. W., Richmond, R. K., Sargent, D. F. and Richmond, T. J. (1997). Crystal structure of the nucleosome core particle at 2.8 A resolution. *Nature* **389**, 251-260.

Matsumoto, K., Nagata, K., Okuwaki, M. and Tsujimoto, M. (1999). Histone- and chromatin-binding activity of template activating factor-I. *FEBS Lett.* **463**, 285-288.

Meshorer, E., Yellajoshula, D., George, E., Scambler, P. J., Brown, D. T. and Misteli, T. (2006). Hyperdynamic plasticity of chromatin proteins in pluripotent embryonic stem cells. *Dev. Cell* **10**, 105-116.

Misteli, T., Gunjan, A., Hock, R., Bustin, M. and Brown, D. T. (2000). Dynamic binding of histone H1 to chromatin in living cells. *Nature* **408**, 877-881.

Miyaji-Yamaguchi, M., Kato, K., Nakano, R., Akashi, T., Kikuchi, A. and Nagata, K. (2003). Involvement of nucleocytoplasmic shuttling of yeast Nap1 in mitotic progression. *Mol. Cell. Biol.* **23**, 6672-6684.

Miyaji-Yamaguchi, M., Okuwaki, M. and Nagata, K. (1999). Coiled-coil structure-mediated dimerization of template activating factor-I is critical for its chromatin remodeling activity. *J. Mol. Biol.* **290**, 547-557.

Muto, S., Senda, M., Akai, Y., Sato, L., Suzuki, T., Nagai, R., Senda, T. and Horikoshi, M. (2007). Relationship between the structure of SET/TAF-Ibeta/INHAT and its histone chaperone activity. *Proc. Natl. Acad. Sci. USA* **104**, 4285-4290.

Nagata, K., Saito, S., Okuwaki, M., Kawase, H., Furuya, A., Kusano, A., Hanai, N., Okuda, A. and Kikuchi, A. (1998). Cellular localization and expression of template-activating factor I in different cell types. *Exp. Cell Res.* **240**, 274-281.

Okuwaki, M., Kato, K. and Nagata, K. (2010). Functional characterization of human nucleosome assembly protein 1-like proteins as histone chaperones. *Genes Cells* **15**, 13-27.

Okuwaki, M., Kato, K., Shimahara, H., Tate, S. and Nagata, K. (2005). Assembly and disassembly of nucleosome core particles containing histone variants by human nucleosome assembly protein I. *Mol. Cell. Biol.* **25**, 10639-10651.

Park, Y. J., Chodaparambil, J. V., Bao, Y., McBryant, S. J. and Luger, K. (2005). Nucleosome assembly protein 1 exchanges histone H2A-H2B dimers and assists nucleosome sliding. *J. Biol. Chem.* **280**, 1817-1825.

Park, Y. J. and Luger, K. (2006). The structure of nucleosome assembly protein 1. *Proc. Natl. Acad. Sci. USA* **103**, 1248-1253.

Phair, R. D., Scaffidi, P., Elbi, C., Vecerova, J., Dey, A., Ozato, K., Brown, D. T., Hager, G., Bustin, M. and Misteli, T. (2004). Global nature of dynamic protein-chromatin interactions in vivo: three-dimensional genome scanning and dynamic interaction networks of chromatin proteins. *Mol. Cell. Biol.* **24**, 6393-6402.

Raghuram, N., Carrero, G., Th'ng, J. and Hendzel, M. J. (2009). Molecular dynamics of histone H1. *Biochem. Cell Biol.* **87**, 189-206.

Rochman, M., Postnikov, Y., Correll, S., Malicet, C., Wincovitch, S., Karpova, T. S., McNally, J. G., Wu, X., Bubunenko, N. A., Grigoryev, S. et al. (2009). The interaction of NSBP1/HMGN5 with nucleosomes in euchromatin counteracts linker histone-mediated chromatin compaction and modulates transcription. *Mol. Cell* **35**, 642-656.

Saeki, H., Ohsumi, K., Aihara, H., Ito, T., Hirose, S., Ura, K. and Kaneda, Y. (2005). Linker histone variants control chromatin dynamics during early embryogenesis. *Proc. Natl. Acad. Sci. USA* **102**, 5967-5702.

Shintomi, K., Iwabuchi, M., Saeki, H., Ura, K., Kishimoto, T. and Ohsumi, K. (2005). Nucleosome assembly protein-1 is a linker histone chaperone in Xenopus eggs. *Proc. Natl. Acad. Sci. USA* **102**, 8210-8215.

Sprague, B. L., Pego, R. L., Stavreva, D. A. and McNally, J. G. (2004). Analysis of binding reactions by fluorescence recovery after photobleaching. *Biophys. J.* **86**, 3473-3495.

Tagami, H., Ray-Gallet, D., Almouzni, G. and Nakatani, Y. (2004). Histone H3.1 and H3.3 complexes mediate nucleosome assembly pathways dependent or independent of DNA synthesis. *Cell* **116**, 51-61.

Th'ng, J. P., Sung, R., Ye, M. and Hendzel, M. J. (2005). H1 family histones in the nucleus. Control of binding and localization by the C-terminal domain. *J. Biol. Chem.* **280**, 27809-27814.

Tremethick, D. J. (2007). Higher-order structures of chromatin: the elusive 30 nm fiber. *Cell* **128**, 651-654.

Trojer, P., Zhang, J., Yonezawa, M., Schmidt, A., Zheng, H., Jenuwein, T. and Reinberg, D. (2009). Dynamic histone H1 isotype 4 methylation and demethylation by histone lysine methyltransferase G9a/KMT1C and the Jumonji domain-containing JMJD2/KDM4 proteins. *J. Biol. Chem.* **284**, 8395-8405.

Vaquero, A., Scher, M., Lee, D., Erdjument-Bromage, H., Tempst, P. and Reinberg, D. (2004). Human SirT1 interacts with histone H1 and promotes formation of facultative heterochromatin. *Mol. Cell* **16**, 93-105.

Wisniewski, J. R., Zougman, A., Kruger, S. and Mann, M. (2007). Mass spectrometric mapping of linker histone H1 variants reveals multiple acetylations, methylations, and phosphorylation as well as differences between cell culture and tissue. *Mol. Cell Proteomics* **6**, 72-87.

Yellajoshyula, D. and Brown, D. T. (2006). Global modulation of chromatin dynamics mediated by dephosphorylation of linker histone H1 is necessary for erythroid differentiation. *Proc. Natl. Acad. Sci. USA* **103**, 18568-18573.

JOURNAL OF INTERFERON & CYTOKINE RESEARCH
Volume 31, Number 11, 2011

DOI: 10.1089/jir.2010.0132

Interferon-Inducible Antiviral Protein MxA Enhances Cell Death Triggered by Endoplasmic Reticulum Stress

Akiko Numajiri Haruki,* Tadasuke Naito,* Tomomi Nishie, Shoko Saito, and Kyosuke Nagata

Human myxovirus resistance gene A (MxA) is a type I interferon-inducible protein and exhibits the antiviral activity against a variety of RNA viruses, including influenza virus. Previously, we reported that MxA accelerates cell death of influenza virus-infected cells through caspase-dependent and -independent mechanisms. Similar to other viruses, influenza virus infection induces endoplasmic reticulum (ER) stress, which is one of cell death inducers. Here, we have demonstrated that MxA enhances ER stress signaling in cells infected with influenza virus. ER stress-induced events, such as expression of *BiP* mRNA and processing of *XBP1* mRNA, were upregulated in cells expressing MxA by treatment with an ER stress inducer, tunicamycin (TM), as well as influenza virus infection. TM-induced cell death was also accelerated by MxA. Furthermore, we showed that MxA interacts with BiP and overexpression of BiP reduces MxA-promoted ER stress signaling. Because cell death in virus-infected cells is one of ultimate anti-virus mechanisms, we propose that MxA-enhanced ER stress signaling is a part of the antiviral activity of MxA by accelerating cell death.

Introduction

THE INTERFERON (IFN) SYSTEM plays a central role in host defense against virus infection. IFN-inducible proteins exhibit antiviral roles through translation inhibition, viral RNA metabolism, and so on (García-Sastre and Biron 2006; Sadler and Williams 2008). Furthermore, it was shown that cell death of virus-infected cells, which is one of the ultimate host defense systems, was promoted by some of IFN-inducible proteins, including human myxovirus resistance gene A (MxA) protein (MxA) (Castelli and others 1997; Gil and others 2002; Numajiri and others 2006). MxA is one of the major IFN-inducible proteins and plays a distinct role in the IFN type I-mediated response in cells infected with a variety of viruses such as orthomyxovirus, paramyxovirus, rhabdovirus, togavirus, bunyavirus, coxsackie virus, and hepatitis B virus (Haller and others 2007; Sadler and Williams 2008). A variety of antiviral activities are associated with MxA, although the exact action mechanism is unclear. The anti-viral activity appears to vary depending on the nature of the infecting viruses (Haller and others 2007; Sadler and Williams 2008). MxA may also promote cell death infected with influenza virus (Numajiri and others 2006).

Virus infection causes destruction of infected cells, and induces apoptosis. Most cells undergo cell death while also producing pro-inflammatory cytokines to spread the alarm to their neighboring cells. In turn, viruses employ strategies to regulate the mitochondrial checkpoint for apoptosis, in particular by altering the balance of pro-apoptotic and pro-survival protein levels, by either producing pro-survival inhibitors to lead to cellular death or expressing proteins to maintain cellular survival such as viral Bcl-2 homologs (Galluzzi and others 2008; Postigo and Ferrer 2009).

Several viral proteins have been shown to induce apoptosis through direct effect on mitochondrial compartment or cellular factors. The influenza virus PB1-F2 protein enhances cell death by interaction with ANT3 and VDAC1 proteins at inner and outer mitochondrial membranes, respectively (Zamarin and others 2005). The transforming growth factor-β (TGF-β) activity increases in cells infected with influenza virus. Viral neuraminidase (NA) activates TGF-β, a known inducer of apoptosis, by elimination of sialic acid residues attached to carbohydrates on the latent TGF-β binding protein, which is associated with pro-TGF-β (Schultz-Cherry and Hinshaw 1996; Morris and others 1999). This allows the subsequent removal of the carbohydrate, a pre-determinant for the proteolytic cleavage of pro-TGF-β and release of the active molecule. Viral NS1 and M1 proteins are implicated in modulating apoptotic responses in infected cells. NS1 appears to downregulate apoptosis, although it can induce apoptosis when expressed from a plasmid in absence of virus replication (Morris and others 2002). M1 binds directly with and may inhibit caspase-8 (Zhirnov and others 1999; Timofeeva and others 2001). However, M1 can induce apoptosis in cells expressing this protein from a plasmid. In addition, efficient viral

Department of Infection Biology, Graduate School of Comprehensive Human Sciences, University of Tsukuba, Tsukuba, Japan.
*These two authors contributed to this work equally.

mRNA synthesis has also been shown to be related with apoptosis induction (Stray and Air 2001).

Recently, it was reported that endoplasmic reticulum (ER) stress signaling is triggered and/or regulated by viruses (He 2006). The accumulation of unfolded proteins in the lumen of ER induces a coordinated adaptive program called unfolded protein response (UPR). UPR increases expression of molecular chaperones such as Grp94 and Grp78/BiP to facilitate proper protein folding. Recent studies showed that a variety of viral proteins trigger BiP expression during virus infection, although the effect of upregulation of BiP on virus replication is not fully understood (Jordan and others 2002; Limjindaporn and others 2009). Upon ER stress, activated inositol-requiring enzyme 1 (IRE1) initiates an unconventional splicing of *XBP1* mRNA precursor to excise its unusual intron. The spliced *XBP1* mRNA is efficiently translated into an active basic leucine zipper transcription factor to upregulate transcription of UPR genes (He 2006). Despite of UPR, unfolded proteins often accumulate and can cause apoptosis. C/EBP homologous protein (CHOP), one of the UPR downstream effectors, is a dominant-negative type inhibitor of CCAAT/enhancer-binding proteins. CHOP-mediated apoptosis is known to be coupled with a pathway that suppresses expression of Bcl-2 and intracellular glutathione and the increase of free radicals. The exact downstream target(s) of CHOP remains unclarified (He 2006). It is proposed that IRE1 plays a role in ER stress-mediated apoptosis by the interaction with tumor necrosis factor receptor-associated factor-2, which is thought to be required for the activation of procaspase-12. Activated caspase-12 cleaves procaspase-9 to generate active caspase-9, and consequently leads to activation of the caspase cascade (Urano and others 2000; Rao and others 2002a).

After influenza virus infection, BiP interacts with newly synthesized viral hemagglutinin (HA) and NA proteins (Hurtley and others 1989; Hogue and Nayak 1992). Folding and oligomerization of both proteins are normally efficient, but misfolded HA and NA are generated spontaneously in infected cells, and associate with BiP and then retain in ER. BiP-associated misfolded HA is not transported to the plasma membrane but sustained as complexes in ER for a long period before degradation. These accumulated viral proteins make BiP released from PERK, ATF6, and IRE1, which subsequently activate UPR.

In this study, we have shown that antiviral protein MxA enhances ER stress-mediated cell death after influenza virus infection. Previously, we reported that MxA accelerates cell death induced by influenza viral infection (Mibayashi and others 2002; Numajiri and others 2006). MxA promotes both caspase-dependent and caspase-independent cell death. However, the detailed stimulatory mechanism of cell death induced by MxA is unclear. We found that MxA can enhance transcription of UPR target genes. Furthermore, we have shown that MxA functionally interacts with ER chaperone BiP to promote UPR and apoptosis. Taken altogether, we propose that the cell death promotion activity of MxA plays a role for its antiviral activity.

Materials and Methods

Cells, virus infection, and transfection

Swiss mouse 3T3 cell lines, Swiss3T3-Neo and Swiss3T3-MxA cells (Staeheli and others 1986), were kindly provided by Drs. Haller and Kochs and maintained in Dulbecco's modified Eagle's medium supplemented with 10% fetal bovine serum (FBS). HeLa cells were maintained in minimal essential medium supplemented with 10% FBS. All cells were maintained at 37°C in a 5% CO_2 incubator. For infection, monolayer cultures of Swiss3T3-Neo and Swiss3T3-MxA cells in 100-mm-diameter dishes were washed twice with serum-free medium, and then infected with influenza A/PR/8 virus at a multiplicity of infection (MOI) of 10 plaque forming unit (PFU) per cell. After virus adsorption at 37°C for 1 h, the cells were washed with serum free medium and then incubated with the fresh medium at 37°C for indicated periods. Transfection of HeLa and HEK293T cells with plasmids was carried out by the standard calcium phosphate method or using transfection reagent TransIT (Mirus).

Chemical compounds

Tunicamycin (TM) and salubrinal (Sal) were purchased from Calbiochem. Brefeldin A (BFA) was purchased from Wako. These compounds were dissolved in dimethlysulfoxide.

Construction of plasmid vectors

An eukaryotic expression vector, pCHA-MxA, was constructed previously (Mibayashi and others 2002). To construct pCHA-MxA mutant vectors, pCHA-MxAΔC241 and pCHA-MxAΔC574, the insert cDNAs were amplified by polymerase chain reaction (PCR), digested with *Mlu*I and *Afl*II, and subloned into *Mlu*I- and *Afl*II-digested pCHA vector. PCR amplification was performed using pCHA-MxA as template and primers as follows: 5′-GGACGCGTATGGTTGTTTCCGAA GTGGAC-3′ for pCHA-MxAΔC241 and pCHA-MxAΔC574, 5′-GGCTTAAGTCATTAGACCACCACCAGGCTGAT-3′ for pCHA-MxAΔC241, and 5′-GGCTTAAGTCATTAGGAAGA GTCTGTTGCCGA-3′ for pCHA-MxAΔC574. Plasmids of pCHA-MxAΔC and pCHA-MxAΔN were prepared as described previously (Numajiri and others 2006).

Plasmid vectors for luciferase assays, pGL3-GRP78P(-132)-luc (Yoshida and others 1998) and p5xATF6GL3 (Wang and others 2000) designated ER stress response element (ERSE) and UPR element (UPRE) reporters, respectively, were kind gifts from Drs. Mori and Prywes, respectively. For construction of mammalian expression vector for mouse BiP, a cDNA fragments corresponding to BiP ORF with a FLAG tag at its N-terminus was amplified by reverse transcriptase (RT)-PCR with primers 5′ GCGGATCCCCGCCACCATG ACTACAAGGATGACGACAAGATGATGAAGTTCACTG TGGTGGC 3′ and 5′ GCGGATCCCTACAACTCATCTTT TTCTGATGTATC 3′ and mouse total RNA as template. PCR product was digested with *Bam*HI (TOYOBO), and inserted into the *Bam*HI site of pcDNA3 (Invitrogen) to create pcDNA3-FLAG-BiP. The details for the generation of the plasmid for hNAP-1 (Okuwaki and others 2010) will be described elsewhere.

Reverse transcriptase–polymerase chain reaction

Total RNA was isolated from Swiss3T3-Neo and Swiss3T3-MxA cells by the guanidine method. cDNA was synthesized from total RNA (0.5–2 μg) using Superscript II reverse transcriptase (RT; Invitrogen) and oligo-dT_{20} primer. PCR was performed using the above cDNAs (1/20, vol/vol) as template and a set of specific primers by pre-determined

PCR cycles, under which PCR products are semi-logarithmically amplified. Primer sequences used in this study were as follows: for mouse (m) *BiP*, 5′ AAGGTCTATGAAGGTG AACGACCCC 3′ and 5′ GACCCCAAGACATGTGAGCA ACTGC 3′; for m*XBP1*, 5′ CACGCTTGGGAATGGACACG 3′ and 5′ GATGAGGTCCCCACTGACAG 3′; for m*CHOP*, 5′ GCACGCGTATGGCAGCTGAGTCCCTGC 3′ and 5′ GCG ATATCATGCTTGGTGCAGGCTGA 3′; and for m*β-actin*, 5′ ATGGGTCAGAAGGACTCCTATGTGGG 3′ and 5′ CTAG AAGCACTTGCGGTGCACGATG 3′. The PCR products were separated on 1% agarose gel electrophoresis for *BiP*, *CHOP*, and *β-actin*, and 8% polyacrylamide gel electrophoresis (PAGE) for *XBP1*, and observed by staining with EtBr.

Real-time RT-PCR

Total RNA extraction was performed with RNeasy minikit (Qiagen), and reverse-transcribed into cDNAs by using a ReverTra Ace and oligo(dT) primer (TOYOBO). The amounts of cDNAs for *CHOP* and *β-actin* were quantified using Fast Start SYBR Green Master (Roche).

Trypan blue dye exclusion assay

Typan blue dye exclusion assays were carried out as previously described (Numajiri and others 2006). Swiss3T3-Neo and Swiss3T3-MxA cells in 60-mm-diameter dishes were treated with TM (SIGMA). After cell death induction for indicated periods, both adherent and floating cells were collected together by centrifugation. The cells were resuspend in 0.02% trypan blue (SIGMA) in phosphate-buffered saline (PBS), and dead and living cells were counted using hemocytometer.

Fluorescence-activated cell sorter analysis

Cells were treated as indicated in figure legends, collected, and then stained with propidium iodide (5 μg/mL). Fluorescence-activated cell sorting (FACS) analysis was performed using FACSCalibur instrument (BD biosciences) using CellQuest software.

Luciferase assay

The luciferase activity was determined using commercially available reagents (Promega) according to the manufacturer's protocol. The relative luciferase activity was measured for 10 s with a luminometer. The *Firefly* luciferase activity was normalized as that relative to the *Renilla* luciferase activity derived from a co-transfected control plasmid pRL-SV40 (Promega).

Indirect immunofluorescence assay

The double immunostaining of HA-MxA, FLAG-BiP, and PB1 was carried out at room temperature as follows: HeLa cells grown on glass coverslips in culture dishes were transfected with plasmid DNAs. After 24 h post transfection, the cells were infected with influenza A/PR/8 virus at MOI of 10 PFU per cell according to the protocol described above. After 8 h postinfection (hpi), cells were washed, fixed with PBS containing 4% paraformaldehyde, and then permeabilized with PBS containing 0.5% Triton X-100. The coverslips were soaked in TBS-T [25 mM Tris-HCl (pH 7.9), 137 mM NaCl, and 3 mM KCl, 0.1% Tween 20] containing 5% skim milk for 30 min. Cells were then incubated for 1 h with primary antibodies: mouse anti-HA clone 12CA5 (1:250; Roche), rat anti-HA clone 3F10 (1:3,000; Roche), rabbit anti-PB1 antibodies (1:500) (Naito and others 2007), or mouse anti-FLAG M2 (1:3,000; SIGMA) monoclonal antibodies. After washing with PBS containing 0.1% NP-40, the cells were incubated for 30 min with secondary antibodies: Alexa Fluor 488 goat anti-mouse (1:2,000; Molecular Probe, A11029), Alexa Fluor 568 goat anti-rabbit (1:2,000; Molecular Probe, A11011), and Alexa Fluor 633 goat anti-rat (1:2,000; Molecular Probe, A21094) antibodies. Coverslips were washed with PBS containing 0.1% NP-40, and incubated for 10 min with 10 mM 4′,6′-diamido-2-phenylindole dihydrochloride. After washing with PBS containing 0.1% NP-40, the coverslips were mounted on slide glasses. The cells were then observed under a fluorescence microscope (Carl Zeiss).

Immunoprecipitation assays

Transfected cells were washed with PBS and collected by centrifugation. Cells were re-suspended in IP buffer [20 mM Tris-HCl (pH 7.9), 150 mM NaCl, 30 mM KCl, 1 mM EDTA, and 0.1% NP-40]. After sonication, homogenates were centrifuged at 10,000 rpm at 4°C for 10 min. The supernatant was recovered and used for immunoprecipitation assays. Cell extracts were mixed with mouse anti-MxA KM1124 (Kyowa Medex) or mouse anti-FLAG M2 (SIGMA) antibodies and incubated at 4°C for 2 h. Immunocomplexes were recovered by the addition of protein A Sepharose Fast Flow beads (GE Healthcare). The beads were washed 3 times with IP buffer. Immunoprecipitated proteins were separated by sodium dodecyl sulfate–10% PAGE and subjected to western blot analyses using anti-HA clone 3F10 and anti-FLAG M2 antibodies.

Results

ER stress-mediated cell death is promoted by MxA

Previously, we reported that MxA has the cell death promotion activity (Mibayashi and others 2002; Numajiri and others 2006). After influenza virus infection, cells expressing MxA died faster than MxA-negative cells. Here, we have addressed how the cell death, after influenza virus infection, is triggered in cells expressing MxA. It is well established that one of the triggers of the cell death upon viral infection is the ER stress-induced cell death mechanism (He 2006). Indeed, *BiP* mRNA accumulates after influenza virus infection (Maruoka and others 2003). Thus, we first examined the expression level of *BiP* mRNA in cells expressing MxA upon influenza virus infection. In this study, we used Swiss3T3-MxA, a previously established cell line expressing MxA constitutively (Staeheli and others 1986), because MxA is IFN-inducible in certain cells and the addition of IFN may affect other IFN-related cell death/survival pathways. The level of *BiP* mRNA was upregulated in cells expressing MxA at 3 hpi (Fig. 1A). In addition, splicing of *XBP1* mRNA, an event closely correlated with ER stress, was also enhanced in cells expressing MxA at 3 hpi. These results showed that MxA enhances ER-mediated stress signaling after influenza virus infection.

Next, we examined whether MxA enhances ER stress-mediated stress signaling leading to cell death promotion upon stimuli other than influenza virus infection, because

influenza virus infection may induce a variety of cellular signaling pathways. We utilized an ER stress inducer, TM, which inhibits N-linked glycosylation and thereby causes protein accumulation in ER. Swiss3T3-MxA and Swiss3T3-Neo cells negative in MxA expression were treated with 0.5 μg/mL of TM, and then subjected to trypan blue dye exclusion assays. While TM induces cell death in both MxA-positive and control cells, the number of dead cells was 8–10 times greater in MxA-positive cells (Fig. 1B). More than 70% of MxA-positive cells died at 48 h after TM treatment.

In parallel, we examined whether caspase-12 activation is further enhanced by MxA. Caspase-12 is activated specifically in cells suffered from ER stress (Morishima and others 2002) and functions as the initiator caspase in response to a toxic insult to ER, such as treatment with TM or calcium ionophores (Nakagawa and others 2000). Treatment of cells with TM resulted in the processing of procaspase-12 (48 kDa) (Fig. 1C). We found that the procaspase-12 level decreased, whereas one of cleaved products increased. We could not detect the prodomain, because caspase-12 antibody used (SIGMA; C7611) here does not recognize the prodomain. Key finding is that the cleavage of procaspase-12 was enhanced in MxA-positive cells upon TM treatment. This result suggests that MxA promotes ER stress-mediated cell death after TM treatment.

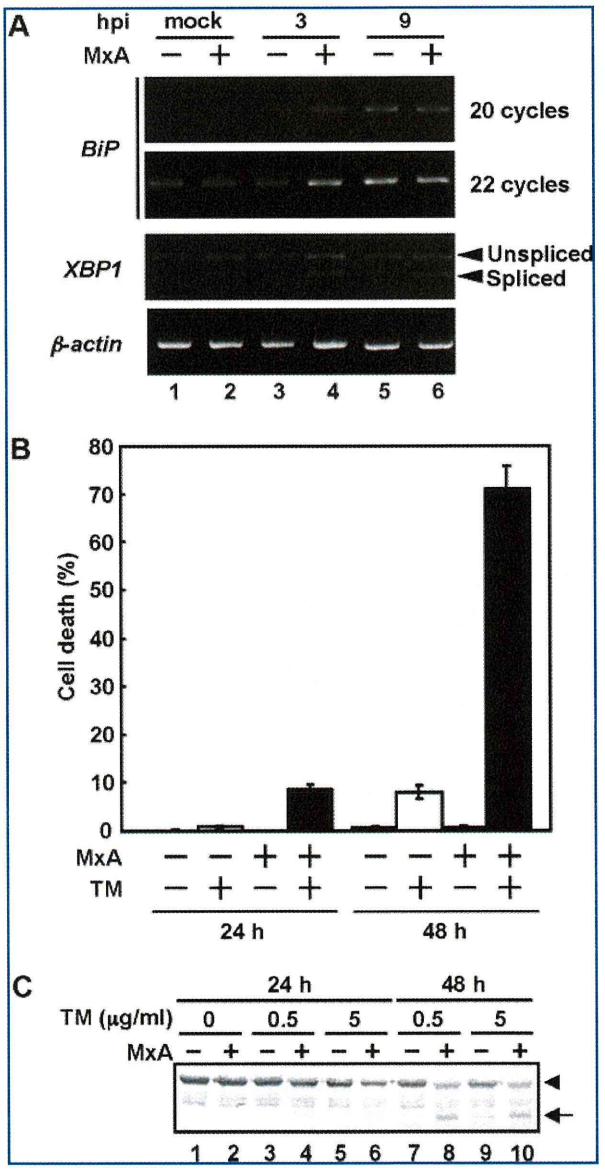

Promotion of apoptosis mediated by MxA is repressed in the presence of a selective inhibitor of ER stress response

MxA was involved in apoptosis acceleration induced by TM (Fig. 1B, C). However, a rapid accumulation of proteins within ER and collapse of Golgi stacks by treatment of TM or BFA may induce various apoptosis pathways beside ER stress-induced cell death. We examined whether MxA specifically functions in UPR-mediated apoptosis by using a selective inhibitor, Sal. Sal blocks dephosphorylation of eukaryotic translation initiation factor 2 subunit α and protects cells from ER stress-induced apoptosis (Boyce and others 2005).

To determine the effect of Sal on ER stress pathway-specific apoptosis acceleration by MxA, we carried out FACS analyses. As shown in Fig. 2A, we confirmed using the FACS method that cell death is induced by TM treatment and further promoted by MxA. Previously, we showed that cell death is enhanced in MxA-expressing cells when cells were treated with cycloheximide (CHX) or ultraviolet irradiation (Numajiri and others 2006). In this report, we examined the impact of Sal on BFA-induced stress condition (Fig. 2B). Cell death was induced by BFA, and enhanced in cells expressing of MxA. Sal suppressed BFA-induced apoptosis, to some extent, not only in MxA-negative cells, but also in MxA-positive cells. These results suggest that apoptosis acceleration by MxA, at least in part, is caused through ER stress signal pathway.

FIG. 1. Cell death is stimulated by TM in cells expressing MxA. **(A)** MxA enhances ER stress caused by influenza virus. Swiss3T3-Neo and Swiss3T3-MxA cells were infected with influenza virus at MOI of 10. After incubation for 3 and 9 h, cells were collected, and the DNA fragment corresponding to *BiP* mRNA was amplified from total RNA by RT-PCR. Resulting products were subjected to 1% agarose gel electrophoresis for *BiP* mRNA (*upper 2 panels*) and *β-actin* mRNA (*lower*) or 8% PAGE for *XBP1* mRNA (*middle*). Unspliced and spliced forms of *XBP1* mRNA were indicated by *arrowheads*. **(B)** Dye exclusion assay. Swiss3T3-Neo (*open columns*) and Swiss3T3-MxA (*filled columns*) cells were treated with TM (0.5 μg/mL). After incubation for 24 and 48 h under cell death induction, cells were collected and subjected to trypan blue dye exclusion assays. **(C)** Cleavage of procaspase-12 upon TM treatment. Swiss3T3-Neo and Swiss3T3-MxA cells were treated with TM (0.5 or 5 μg/mL). After incubation for 24 and 48 h under cell death induction, cells were collected and subjected to western blot analyses with anti-caspase-12 antibody (SIGMA). Procaspase-12 and cleaved forms were indicated by *arrowhead* and *arrow*, respectively. TM, tunicamycin; ER, endoplasmic reticulum; MOI, multiplicity of infection; RT-PCR, reverse transcriptase–polymerase chain reaction.

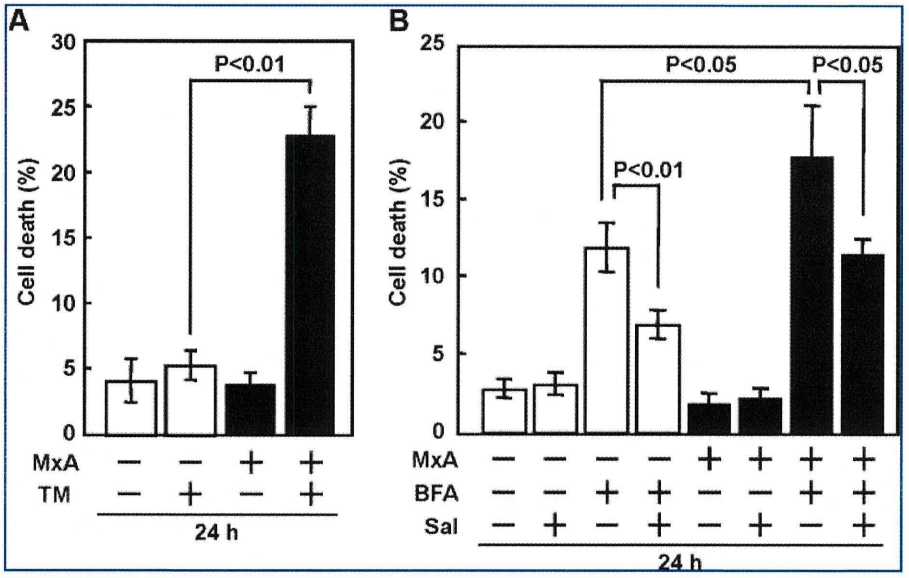

FIG. 2. Sal, a selective ER stress inhibitor suppresses apoptosis accelerated by MxA. **(A)** Swiss3T3-Neo (*open columns*) and Swiss3T3-MxA (*filled columns*) cells were treated with TM (0.5 μg/mL). After incubation for 24 h, cells were collected and subjected to FACS analysis. **(B)** Effect of Sal on MxA-induced cell death. Swiss3T3-Neo (*open columns*) and Swiss3T3-MxA (*filled columns*) cells were treated with 50 μM BFA in the presence or absence of 15 μM Sal. After incubation for 24 h, cells were collected and subjected to FACS analysis. Data were presented as means with standard deviation from 3 independent experiments. FACS, fluorescence-activated cell sorting; BFA, Brefeldin A; Sal, Salubrinal.

MxA accelerates UPR after TM treatment

We next examined whether UPR signaling induced by TM is also enhanced in cells expressing MxA. To this end, we examined the mRNA expression level of genes under the control of the UPR signaling. Swiss3T3-MxA and Swiss3T3-Neo cells were treated with TM, and the mRNA level was examined by RT-PCR method. After 6 and 3 h in the presence of 0.5 and 2.5 μg/mL TM, respectively, the *BiP* mRNA level was increased in cells expressing MxA (Fig. 3A, compare lane 5 with lane 6, and lane 7 with lane 8). From 3 h after treatment with 0.5 μg/mL TM, the spliced form of *XBP1* mRNA was detected in cells expressing MxA, whereas this occurred from 12 h after treatment with TM in MxA-negative cells (Fig. 3B). One of the known signals coordinated with ER stress-induced apoptosis is the expression of CHOP (He 2006). As shown in Fig. 3C, after the treatment with 0.5 μg/mL TM, only MxA-positive cells expressed *CHOP* mRNA. Increase of mRNA amount of the gene under the control of the UPR pathway was distinct only in the presence of low concentrations of TM (Fig. 3C, lanes 4 and 6). This MxA-mediated enhancement was not observed when cells were treated with 2.5 μg/mL TM. MxA may not affect ER signaling induced by vast amounts of unfolded proteins. Furthermore, we confirmed that the amount of *CHOP* mRNA is upregulated in cells transiently expressing MxA (Fig. 3D). Collectively, these suggest that MxA reduces the threshold level of ER stress sensing.

We determined whether MxA enhances the transcription promoter activity directed by ERSE or UPRE under the control of UPR. We utilized pGL3-GRP78P(-132)-luc and p5xATF6GL3 plasmids to monitor ERSE- and UPRE-dependent promoter activities, respectively (Zhu and others 1997; Yoshida and others 1998; Wang and others 2000). As shown in Fig. 3E, F, MxA enhanced both ERSE- and UPRE-dependent promoter activities in response to TM treatment. This enhancement by MxA was in a dose-dependent manner and was undetectable when a reporter plasmid pGL3-GRP78Pmut that lacks ERSE was used (data not shown). These results suggest that MxA affects the signaling pathway leading to the transcription activation upon ER stress response or UPR.

MxA interacts with BiP

We showed that MxA enhances both ATF6- and IRE1-dependent activation of ER stress responses. BiP, an ER chaperone, is known to bind to and stabilize these ER stress sensors (He 2006). Therefore, we consider the possibility that MxA interacts with BiP, either directly or indirectly, and depletes this chaperone in the ER stress response. Since majorities of BiP are localized inside of ER, while MxA is in the cytoplasm, we assumed that an additional factor(s) is involved in the BiP and MxA interaction. However, it is reported that some of BiP is also localized in the cytoplasm (Buchkovich and others 2009). In fact, cytoplasmic BiP interacts with caspase-7 and caspase-12 to prevent cell death (Rao and others 2002b).

As shown in Fig. 4A, MxA and BiP were co-localized around ER in cells co-expressing both proteins. Furthermore, the localization pattern of MxA and BiP in uninfected cells was similar to that observed in influenza virus-infected cells (compare with Fig. 4A, B). At 9 hpi, PB1 was present in the nucleus and the cytoplasm (Fig. 4B). In the same cell, MxA and BiP were co-localized in ER and cytoplasm.

To examine whether MxA interacts with BiP *in vivo*, we performed immunoprecipitation assays using lysates prepared from cells transfected with expression plasmids for FLAG-BiP and either HA-MxA wild type (wt) or mutants (Fig. 4C). Western blot analyses revealed that HA-MxAwt was co-immunoprecipitated with FLAG-BiP when anti-FLAG antibody was used (Fig. 4C, lane 10). We used human nucleosome assembly protein-1-L1 (hNAP-1), one of cytoplasmic proteins, as negative control for overexpression condition (Fig. 4C, lanes 1 and 8). In addition, we tried to identify an interaction domain on MxA and binding specificity with BiP. MxAΔC574 lacking zinc finger motif bound to BiP but only weakly, and MxAΔN interacted with BiP a

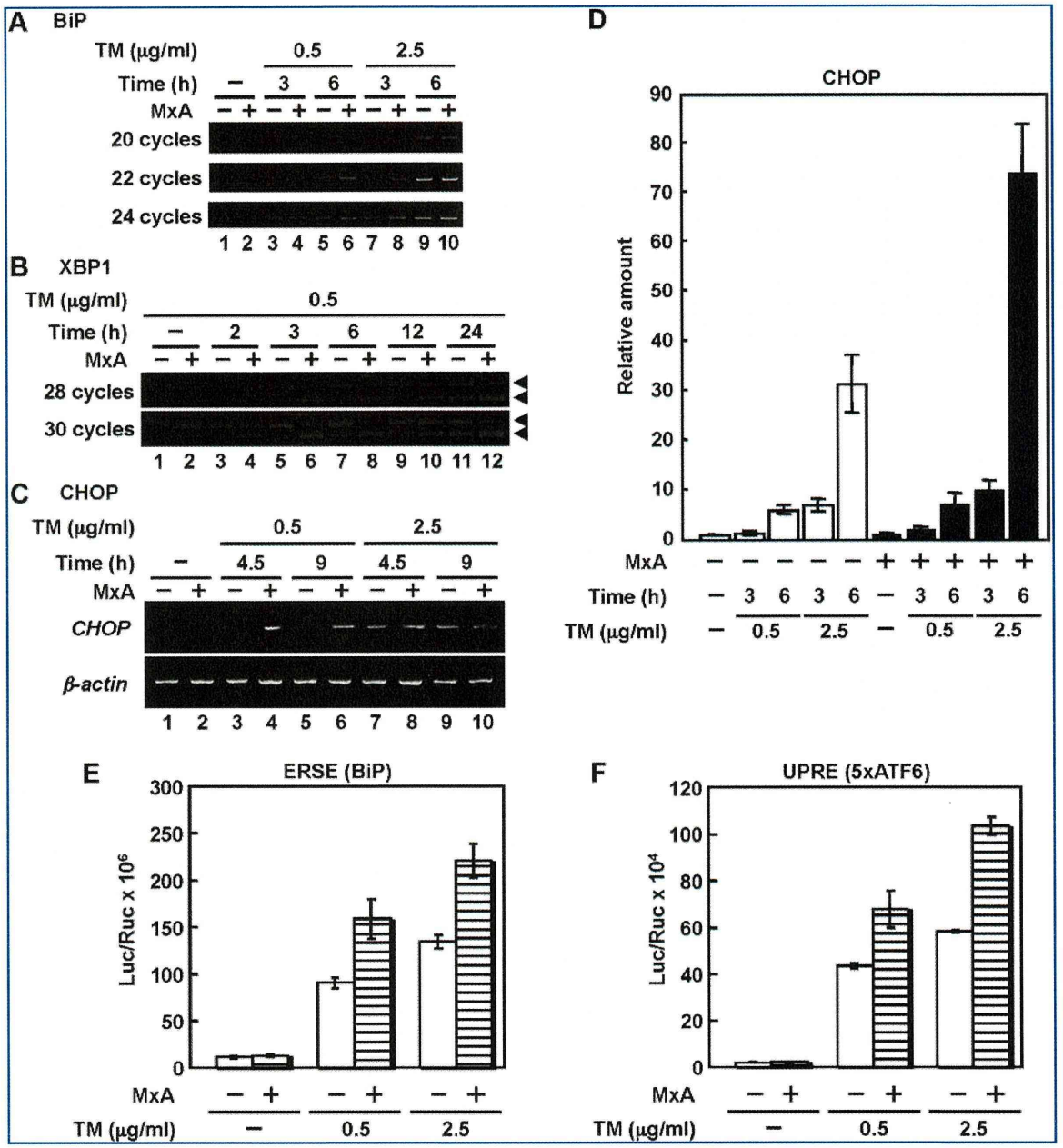

FIG. 3. MxA accelerates UPR after TM treatment. **(A–C)** Swiss3T3-Neo and Swiss3T3-MxA cells were treated with TM at the indicated concentration. After incubation for indicated time periods, cells were collected, and total RNA were subjected to RT-PCR. Amplified DNA fragments were subjected to separation on 1% agarose gel electrophoresis for *BiP* mRNA **(A)** and *CHOP* mRNA **(C)**, or 8% PAGE for *XBP1* mRNA **(B)**. Unspliced and spliced forms of *XBP1* mRNA were indicated by *arrowheads*. **(D)** Quantification of *CHOP* mRNA in MxA-transfected cells using real-time RT-PCR. Swiss3T3 cells were transfected with pCHA or pCHA-MxA plasmid with pBabe-puro. At 24 h post transfection, 2 μg/mL puromycin was added, and cells were grown for further 24 h in growth medium in the presence of 2 μg/mL puromycin. Puromycin-resistant cells were treated with TM at indicated concentrations for 3 and 6 h. **(E, F)** MxA enhances both ERSE and UPRE. HeLa cells were transfected with pGL3-GRP78P(-132)-luc or p5xATF6GL3 in the presence (*striped columns*) or absence (*open columns*) of an expression plasmid encoding MxA, pCHA-MxA (Mibayashi and others 2002). pRL-SV40 encoding the *Renilla* luciferase was used for internal control. At 24 h after transfection, the cells were treated with or without TM (0.5 or 2.5 μg/mL) for 12 h, and *Firefly* and *Renilla* luciferase activities were measured. The *Firefly* result was normalized by the *Renilla* luciferase activity. UPR, unfolded protein response; ERSE, ER stress response element; UPRE, UPR element.

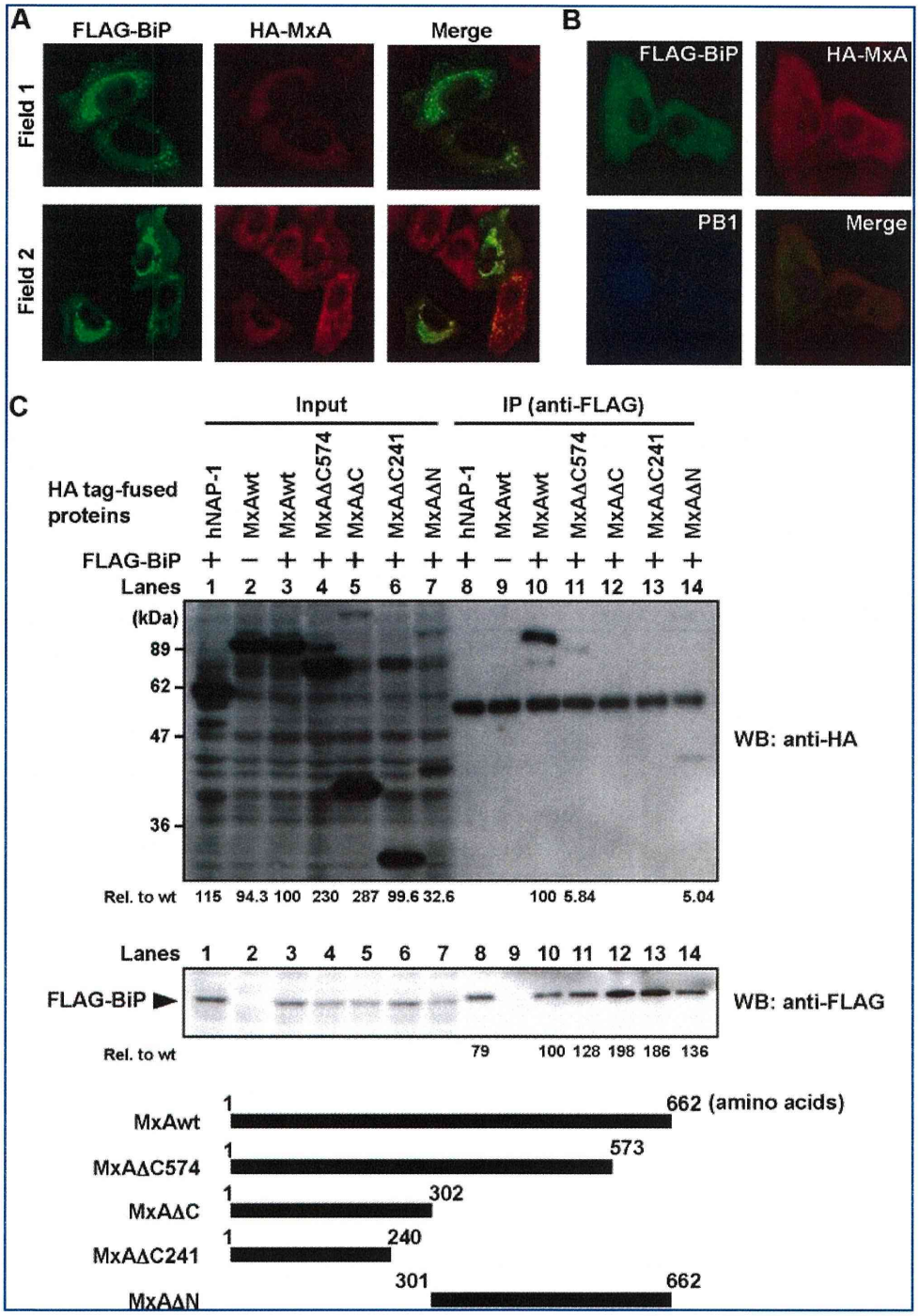

FIG. 4. MxA interacts with BiP. **(A)** Fluorescent immunocytochemical analysis. HeLa cells were transfected with pcDNA-FLAG-BiP and pCHA-MxA, and double-stained with both anti-FLAG and anti-HA antibodies. **(B)** Fluorescent immunocytochemical analysis. HeLa cells were co-transfected with pcDNA3-FLAG-BiP and pCHA-MxA, and at 1 day after transfection, cells were infected with influenza virus at MOI of 10. After incubation for 9 h, cells were collected, and stained with anti-FLAG, anti-HA, and anti-PB1 antibodies. **(C)** Immunoprecipiation assays. HEK293T cells were transfected with pCHA-hNAP-1 (lane 1) or pCHA-MxA mutants (lanes 2–7) in the presence (lanes 1, 3–7) or absence (lane 2) of pcDNA3-FLAG-BiP. Cells were collected at 1 day after transfection, and lysates were subjected to immunoprecipitation assays using anti-FLAG antibody (lanes 8–14). Immunoprecipitated proteins were examined by western blot analyses with anti-HA (*upper panel*) and anti-FLAG antibodies (*lower panel*). Detected protein levels are indicated at the bottom as values relative to those seen in lanes 3 and 10 for the input amount and the immunoprcipitated amount, respectively. MxA mutants used in this assay are schematically illustrated.

little more than MxAΔC574 when compared with the input amounts. However, deletion mutants in the C terminal region, MxAΔC or MxAΔC241 (Fig. 4C, lanes 11 to 14), had virtually no binding capability. Thus, it is quite likely that the region between amino acid positions 301 to 573 of MxA is essential for the binding to BiP. These results indicate that MxA and BiP form a complex around ER. We speculate that this interaction could lead to the activation of ER stress response or the UPR.

BiP suppresses UPR promotion activity of MxA

Finally, we examined whether overexpression of BiP could suppress the ER stress enhancement activity of MxA. We reasoned that either indirect or direct binding of MxA to BiP could be rescued by overexpression of BiP. Reporter gene assays were performed with exogenously overexpressed BiP. Fig. 5A shows that the ER stress response in the absence of TM is not affected by the overexpression of FLAG-BiP. In contrast, in the presence of TM, the activation of ER stress response by MxA was cancelled by overexpressed FLAG-BiP in a dose-dependent manner. Fig. 5B confirmed the expression level of HA-MxA and FLAG-BiP. Thus, it seems likely that ER stress chaperone BiP

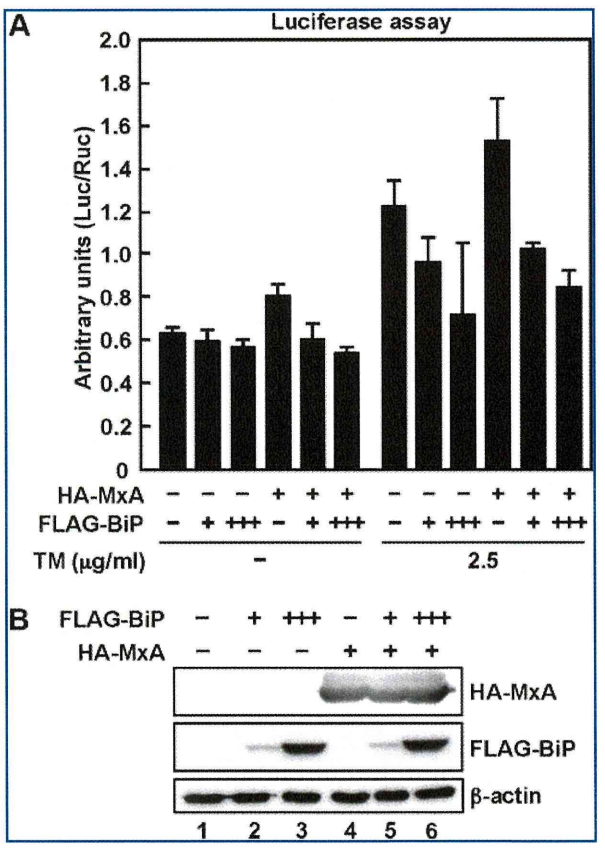

FIG. 5. BiP cancelled UPR promotion activity of MxA. **(A)** Reporter gene assay. HeLa cells were transfected with the reporter plasmid pGL3-GRP78P(-132)-luc with or without pCHA-MxA and pcDNA-FLAG-BiP as described in the figure. At 15 h post transfection, the cells were treated with or without TM (2.5 μg/mL) for 12 h, and the luciferase activity was measured. **(B)** Western blot analyses. Cells treated with TM as shown in **(A)** were subjected to western blot analyses with anti-HA (*upper*), anti-FLAG (*middle*), or anti-β-actin antibodies (*lower*).

cannot be used for its proper role by its depletion through the binding to MxA, either directly or indirectly, on ER membrane. This may reduce the threshold level of ER stress sensing, and thereby promotes the ER stress-induced apoptosis.

Discussion

MxA is an IFN-induced 76 kDa-GTPase that inhibits the multiplication of a variety of RNA viruses, although the exact mechanism of the MxA action is unclear. The antivirus mechanism seems to vary depending on infecting viruses (Schnorr and others 1993; Schneider-Schaulies and others 1994; Landis and others 1998; Gordien and others 2001). When cells expressing MxA are infected with influenza virus, the primary transcription catalyzed by virion-associated viral RNA polymerases occurs at the same level as that in MxA-negative cells (Pavlovic and others 1992). In contrast, viral protein synthesis and genome replication are strongly inhibited (Pavlovic and others 1992). If MxA is forced to be present in the nucleus, nuclear MxA can suppress the influenza virus transcription by interacting with not only the viral polymerase subunit PB2, but also with NP (Turan and others 2004). In addition, we reported that MxA has the cell death promotion activity (Mibayashi and others 2002; Numajiri and others 2006). After influenza virus infection, MxA-positive cells dies faster than MxA-negative cells. We have also shown the caspase-dependent and -independent cell death promotion activity by MxA. It has been reported that the activation of caspase-3 is important during influenza virus proliferation (Queitsch and others 2002). However, the activation level of caspase-3 did not differ between MxA-expressing and MxA-negative cells (Numajiri and others 2006). Therefore, it is possible that MxA could promote cell death without elevation of influenza virus production.

Influenza viruses cause cell death by several mechanisms (Ludwig and others 2006; Sanders and others 2011). Virus infection can induce cell lysis directly, which releases progeny virions and accumulation of a large amount of viral proteins together with potential inflammatory. Promotion of cell death in virus-infected cells may lead to suppression of progeny virion production. The induction of apoptosis might be mediated via intrinsic and/or extrinsic mechanism. It has been shown that viral activation of mitogen-activated protein kinases or their upstream kinases is linked to the onset of apoptosis, and virus infection results in an activation of nuclear factor-κB as an intrinsic pathway. On the other hand, as an extrinsic mechanism of viral apoptosis induction, it has been indicated that the Fas/FasL apoptosis pathway undergoes in a double-stranded RNA activated protein kinase (PKR)-dependent manner in infected cells. The mechanism of viral apoptosis induction might occur via activation of TGF-β, a known apoptosis inducer that is converted from its latent form by NA.

Here, we have addressed the question how MxA promotes cell death after influenza virus infection in light of ER stress signaling. Recent reports suggest that some viruses cause and/or regulate ER stress (Bitko and Barik 2001; Su and others 2002; Tardif and others 2002, 2004; Medigeshi and others 2007). For example, human cytomegalovirus (HCMV) induces splicing of *XBP1* transcript, whereas HCMV suppresses the expression of genes normally regulated by XBP1. It is possible that HCMV utilizes a part of UPR and prevents cell death simultaneously (Isler and others 2005). Dengue

virus envelope protein interacts with BiP and facilitates proper protein folding and protein assembly required for production of progeny virus particles (Limjindaporn and others 2009). In this report, we have shown that MxA enhances ER stress signaling and ER stress-induced cell death upon influenza virus infection. MxA upregulated the transcription level of *BiP* mRNA and the splicing of *XBP1*. MxA also upregulated the transcription level of *CHOP* gene, which is known to be a key mediator for ER stress-induced cell death. Consistent with our findings, CHOP-dependent premature cell death may represent a host defense mechanism to limit viral replication (Medigeshi and others 2007). Previously, we reported that the cell death promotion activity was detected for both MxAwt and MxAΔN, but not for MxΔC in cells treated with CHX as stress inducer. Here, we have shown that the C terminal region on MxA containing oligomelization domain was important in the interaction with BiP. Therefore, similar to the promotion of CHX-induced cell death by MxA, MxA may function as apoptosis accelerator for ER stress-mediated cell death through the same C terminal region.

Previous studies demonstrated that a portion of MxA is localized at membranes belonging to the COP-I-positive subdomain of the smooth ER-Golgi-intermediate compartment (Accola and others 2002; Stertz and others 2006). Furthermore, it has been reported that binding of MxA to viral nucleocapsid protein of La Crosse virus occurs on membranes of the smooth ER-Golgi boundary region and lead to a depletion of the nucleocapsid protein from the viral replication sites (Kochs and others 2002). However, it is presently not clear how MxA interacts with lipid membranes. Anchoring of MxA to distinct membrane compartments may influence the antiviral activity and/or specificity. Recently, Gao and others (2010) reported that the crystal structure of oligomerized stalk region of MxA, which is composed of the middle domain and the GTPase effector domain. The MxA could form a linear oligomers comprised of 13 to 14 dimers. It is not clear how a huge complex of MxA formed through this structure is associated with or incorporated into intracellular membranes. Further studies are needed to clarify details of the connection of MxA-mediated ER stress promotion with antiviral activity.

Acknowledgments

We thank Drs. O. Haller and P. Staeheli (University of Freiburg, Freiburg, Germany), K. Mori (Kyoto University, Kyoto, Japan), and R. Prywes (Columbia University, New York) for their generous gifts of Swiss3T3 and Swiss3T3-MxA cells, and MxA wild-type cDNA, pGL3-GRP78P(-132)-luc, and p5xATF6GL3, respectively. We also thank Dr. Kiong Ho for proofreading the article. This work was supported in part by grants-in-aid from the Ministry of Education, Culture, Sports, Science, and Technology of Japan (T.N. and K.N.).

Author Disclosure Statement

No competing financial interests exist.

References

Accola M, Huang B, Al Masri A, McNiven M. 2002. The antiviral dynamin family member, MxA, tubulates lipids and localizes to the smooth endoplasmic reticulum. J Biol Chem 277:21829–21835.

Bitko V, Barik S. 2001. An endoplasmic reticulum-specific stress-activated caspase (caspase-12) is implicated in the apoptosis of A549 epithelial cells by respiratory syncytial virus. J Cell Biochem 80:441–454.

Boyce M, Bryant KF, Jousse C, Long K, Harding HP, Scheuner D, Kaufman RJ, Ma D, Coen DM, Ron D, Yuan J. 2005. A selective inhibitor of eIF2alpha dephosphorylation protects cells from ER stress. Science 307:935–939.

Buchkovich N, Maguire T, Paton A, Paton J, Alwine J. 2009. The endoplasmic reticulum chaperone BiP/GRP78 is important in the structure and function of the human cytomegalovirus assembly compartment. J Virol 83:11421–11428.

Castelli J, Hassel B, Wood K, Li X, Amemiya K, Dalakas M, Torrence P, Youle R. 1997. A study of the interferon antiviral mechanism: apoptosis activation by the 2-5A system. J Exp Med 186:967–972.

Galluzzi L, Brenner C, Morselli E, Touat Z, Kroemer G. 2008. Viral control of mitochondrial apoptosis. PLoS Pathog 4, e1000018.

Gao S, von der Malsburg A, Paeschke S, Behlke J, Haller O, Kochs G, Daumke O. 2010. Structural basis of oligomerization in the stalk region of dynamin-like MxA. Nature 465:502–506.

García-Sastre A, Biron C. 2006. Type 1 interferons and the virus-host relationship: a lesson in détente. Science 312:879–882.

Gil J, García M, Esteban M. 2002. Caspase 9 activation by the dsRNA-dependent protein kinase, PKR: molecular mechanism and relevance. FEBS Lett 529:249–255.

Gordien E, Rosmorduc O, Peltekian C, Garreau F, Bréchot C, Kremsdorf D. 2001. Inhibition of hepatitis B virus replication by the interferon-inducible MxA protein. J Virol 75:2684–2691.

Haller O, Staeheli P, Kochs G. 2007. Interferon-induced Mx proteins in antiviral host defense. Biochimie 89:812–818.

He B. 2006. Viruses, endoplasmic reticulum stress, and interferon responses. Cell Death Differ 13:393–403.

Hogue BG, Nayak DP. 1992. Synthesis and processing of the influenza virus neuraminidase, a type II transmembrane glycoprotein. Virology 188:510–517.

Hurtley SM, Bole DG, Hoover-Litty H, Helenius A, Copeland CS. 1989. Interactions of misfolded influenza virus hemagglutinin with binding protein (BiP). J Cell Biol 108:2117–2126.

Isler J, Skalet A, Alwine J. 2005. Human cytomegalovirus infection activates and regulates the unfolded protein response. J Virol 79:6890–6899.

Jordan R, Wang L, Graczyk T, Block T, Romano P. 2002. Replication of a cytopathic strain of bovine viral diarrhea virus activates PERK and induces endoplasmic reticulum stress-mediated apoptosis of MDBK cells. J Virol 76:9588–9599.

Kochs G, Janzen C, Hohenberg H, Haller O. 2002. Antivirally active MxA protein sequesters La Crosse virus nucleocapsid protein into perinuclear complexes. Proc Natl Acad Sci U S A 99:3153–3158.

Landis H, Simon-Jödicke A, Klöti A, Di Paolo C, Schnorr J, Schneider-Schaulies S, Hefti H, Pavlovic J. 1998. Human MxA protein confers resistance to Semliki Forest virus and inhibits the amplification of a Semliki Forest virus-based replicon in the absence of viral structural proteins. J Virol 72:1516–1522.

Limjindaporn T, Wongwiwat W, Noisakran S, Srisawat C, Netsawang J, Puttikhunt C, Kasinrerk W, Avirutnan P, Thiemmeca S, Sriburi R, Sittisombut N, Malasit P, Yenchitsomanus P. 2009. Interaction of dengue virus envelope protein with endoplasmic reticulum-resident chaperones facilitates dengue virus production. Biochem Biophys Res Commun 379:196–200.

Ludwig S, Pleschka S, Planz O, Wolff T. 2006. Ringing the alarm bells: signalling and apoptosis in influenza virus infected cells. Cell Microbiol 8:375–386.

Maruoka S, Hashimoto S, Gon Y, Nishitoh H, Takeshita I, Asai Y, Mizumura K, Shimizu K, Ichijo H, Horie T. 2003. ASK1 regulates influenza virus infection-induced apoptotic cell death. Biochem Biophys Res Commun 307:870–876.

Medigeshi G, Lancaster A, Hirsch A, Briese T, Lipkin W, Defilippis V, Früh K, Mason P, Nikolich-Zugich J, Nelson J. 2007. West Nile virus infection activates the unfolded protein response, leading to CHOP induction and apoptosis. J Virol 81:10849–10860.

Mibayashi M, Nakad K, Nagata K. 2002. Promoted cell death of cells expressing human MxA by influenza virus infection. Microbiol Immunol 46:29–36.

Morishima N, Nakanishi K, Takenouchi H, Shibata T, Yasuhiko Y. 2002. An endoplasmic reticulum stress-specific caspase cascade in apoptosis. Cytochrome c-independent activation of caspase-9 by caspase-12. J Biol Chem 277:34287–34294.

Morris SJ, Price GE, Barnett JM, Hiscox SA, Smith H, Sweet C. 1999. Role of neuraminidase in influenza virus-induced apoptosis. J Gen Virol 80 (Pt 1):137–146.

Morris SJ, Smith H, Sweet C. 2002. Exploitation of the Herpes simplex virus translocating protein VP22 to carry influenza virus proteins into cells for studies of apoptosis: direct confirmation that neuraminidase induces apoptosis and indications that other proteins may have a role. Arch Virol 147:961–979.

Naito T, Momose F, Kawaguchi A, Nagata K. 2007. Involvement of Hsp90 in assembly and nuclear import of influenza virus RNA polymerase subunits. J Virol 81:1339–1349.

Nakagawa T, Zhu H, Morishima N, Li E, Xu J, Yankner B, Yuan J. 2000. Caspase-12 mediates endoplasmic-reticulum-specific apoptosis and cytotoxicity by amyloid-beta. Nature 403:98–103.

Numajiri A, Mibayashi M, Nagata K. 2006. Stimulus-dependent and domain-dependent cell death acceleration by an IFN-inducible protein, human MxA. J Interferon Cytokine Res 26: 214–219.

Okuwaki M, Kato K, Nagata K. 2010. Functional characterization of human nucleosome assembly protein 1-like proteins as histone chaperones. Genes Cells 15:13–27.

Pavlovic J, Haller O, Staeheli P. 1992. Human and mouse Mx proteins inhibit different steps of the influenza virus multiplication cycle. J Virol 66:2564–2569.

Postigo A, Ferrer P. 2009. Viral inhibitors reveal overlapping themes in regulation of cell death and innate immunity. Microbes Infect 11:1071–1078.

Queitsch C, Sangster TA, Lindquist S. 2002. Hsp90 as a capacitor of phenotypic variation. Nature 417:618–624.

Rao R, Castro-Obregon S, Frankowski H, Schuler M, Stoka V, del Rio G, Bredesen D, Ellerby H. 2002a. Coupling endoplasmic reticulum stress to the cell death program. An Apaf-1-independent intrinsic pathway. J Biol Chem 277:21836–21842.

Rao R, Peel A, Logvinova A, del Rio G, Hermel E, Yokota T, Goldsmith P, Ellerby L, Ellerby H, Bredesen D. 2002b. Coupling endoplasmic reticulum stress to the cell death program: role of the ER chaperone GRP78. FEBS Lett 514:122–128.

Sadler A, Williams B. 2008. Interferon-inducible antiviral effectors. Nat Rev Immunol 8:559–568.

Sanders CJ, Doherty PC, Thomas PG. 2011. Respiratory epithelial cells in innate immunity to influenza virus infection. Cell Tissue Res 343:13–21.

Schneider-Schaulies S, Schneider-Schaulies J, Schuster A, Bayer M, Pavlovic J, ter Meulen V. 1994. Cell type-specific MxA-mediated inhibition of measles virus transcription in human brain cells. J Virol 68:6910–6917.

Schnorr J, Schneider-Schaulies S, Simon-Jödicke A, Pavlovic J, Horisberger M, ter Meulen V. 1993. MxA-dependent inhibition of measles virus glycoprotein synthesis in a stably transfected human monocytic cell line. J Virol 67:4760–4768.

Schultz-Cherry S, Hinshaw VS. 1996. Influenza virus neuraminidase activates latent transforming growth factor beta. J Virol 70:8624–8629.

Staeheli P, Haller O, Boll W, Lindenmann J, Weissmann C. 1986. Mx protein: constitutive expression in 3T3 cells transformed with cloned Mx cDNA confers selective resistance to influenza virus. Cell 44:147–158.

Stertz S, Reichelt M, Krijnse-Locker J, Mackenzie J, Simpson J, Haller O, Kochs G. 2006. Interferon-induced, antiviral human MxA protein localizes to a distinct subcompartment of the smooth endoplasmic reticulum. J Interferon Cytokine Res 26:650–660.

Stray SJ, Air GM. 2001. Apoptosis by influenza viruses correlates with efficiency of viral mRNA synthesis. Virus Res 77:3–17.

Su H, Liao C, Lin Y. 2002. Japanese encephalitis virus infection initiates endoplasmic reticulum stress and an unfolded protein response. J Virol 76:4162–4171.

Tardif K, Mori K, Kaufman R, Siddiqui A. 2004. Hepatitis C virus suppresses the IRE1-XBP1 pathway of the unfolded protein response. J Biol Chem 279:17158–17164.

Tardif K, Mori K, Siddiqui A. 2002. Hepatitis C virus subgenomic replicons induce endoplasmic reticulum stress activating an intracellular signaling pathway. J Virol 76:7453–7459.

Timofeeva TA, Klenk ND, Zhirnov OP. 2001. [Identification of the protease-binding domain in the N-terminal region of the influenza A virus matrix protein M1]. Mol Biol (Mosk) 35:484–491.

Turan K, Mibayashi M, Sugiyama K, Saito S, Numajiri A, Nagata K. 2004. Nuclear MxA proteins form a complex with influenza virus NP and inhibit the transcription of the engineered influenza virus genome. Nucleic Acids Res 32:643–652.

Urano F, Wang X, Bertolotti A, Zhang Y, Chung P, Harding H, Ron D. 2000. Coupling of stress in the ER to activation of JNK protein kinases by transmembrane protein kinase IRE1. Science 287:664–666.

Wang Y, Shen J, Arenzana N, Tirasophon W, Kaufman R, Prywes R. 2000. Activation of ATF6 and an ATF6 DNA binding site by the endoplasmic reticulum stress response. J Biol Chem 275:27013–27020.

Yoshida H, Haze K, Yanagi H, Yura T, Mori K. 1998. Identification of the cis-acting endoplasmic reticulum stress response element responsible for transcriptional induction of mammalian glucose-regulated proteins. Involvement of basic leucine zipper transcription factors. J Biol Chem 273:33741–33749.

Zamarin D, García-Sastre A, Xiao X, Wang R, Palese P. 2005. Influenza virus PB1-F2 protein induces cell death through mitochondrial ANT3 and VDAC1. PLoS Pathog 1:e4.

Zhirnov OP, Konakova TE, Garten W, Klenk H. 1999. Caspase-dependent N-terminal cleavage of influenza virus nucleocapsid protein in infected cells. J Virol 73:10158–10163.

Zhu C, Johansen F, Prywes R. 1997. Interaction of ATF6 and serum response factor. Mol Cell Biol 17:4957–4966.

Address correspondence to:
Prof. Kyosuke Nagata
Department of Infection Biology
Graduate School of Comprehensive Human Sciences
University of Tsukuba
1-1-1 Tennodai
Tsukuba 305-8575
Japan

E-mail: knagata@md.tsukuba.ac.jp

Received 28 September 2010/Accepted 5 July 2011

OPEN ACCESS Freely available online

PLoS one

Tamiflu-Resistant but HA-Mediated Cell-to-Cell Transmission through Apical Membranes of Cell-Associated Influenza Viruses

Kotaro Mori[9], **Takahiro Haruyama**[9¤], **Kyosuke Nagata***

Department of Infection Biology, Faculty of Medicine and Graduate School of Comprehensive Human Sciences, University of Tsukuba, Tsukuba, Japan

Abstract

The infection of viruses to a neighboring cell is considered to be beneficial in terms of evasion from host anti-virus defense systems. There are two pathways for viral infection to "*right next door*": one is the virus transmission through cell-cell fusion by forming syncytium without production of progeny virions, and the other is mediated by virions without virus diffusion, generally designated cell-to-cell transmission. Influenza viruses are believed to be transmitted as *cell-free* virus from infected cells to uninfected cells. Here, we demonstrated that influenza virus can utilize cell-to-cell transmission pathway through apical membranes, by handover of virions on the surface of an infected cell to adjacent host cells. Live cell imaging techniques showed that a recombinant influenza virus, in which the *neuraminidase* gene was replaced with the *green fluorescence protein* gene, spreads from an infected cell to adjacent cells forming infected cell clusters. This type of virus spreading requires HA activation by protease treatment. The cell-to-cell transmission was also blocked by amantadine, which inhibits the acidification of endosomes required for uncoating of influenza virus particles in endosomes, indicating that functional hemagglutinin and endosome acidification by M2 ion channel were essential for the cell-to-cell influenza virus transmission. Furthermore, in the cell-to-cell transmission of influenza virus, progeny virions could remain associated with the surface of infected cell even after budding, for the progeny virions to be passed on to adjacent uninfected cells. The evidence that cell-to-cell transmission occurs in influenza virus lead to the caution that local infection proceeds even when treated with neuraminidase inhibitors.

Citation: Mori K, Haruyama T, Nagata K (2011) Tamiflu-Resistant but HA-Mediated Cell-to-Cell Transmission through Apical Membranes of Cell-Associated Influenza Viruses. PLoS ONE 6(11): e28178. doi:10.1371/journal.pone.0028178

Editor: Ron A. M. Fouchier, Erasmus Medical Center, The Netherlands

Received July 8, 2011; **Accepted** November 2, 2011; **Published** November 30, 2011

Funding: This work was supported in part by a grant-in-aid from the Ministry of Education, Culture, Sports, Science, and Technology of Japan (to KN: #20249025). The funders had no role in study design, data collection and analysis, decision to publish, or preparation of the manuscript. The authors received no additional external funding for this study.

Competing Interests: The authors have declared that no competing interests exist.

* E-mail: knagata@md.tsukuba.ac.jp

[9] These authors contributed equally to this work.

¤ Current address: Central Research Center, AVSS Corporation, Nagasaki, Japan

Introduction

It is generally accepted that viruses, released as *cell-free* virions from an infected cell, transmit to distant cells and tissues. This spreading pathway contributes to wide-ranged diffusion of *cell-free* viruses. However, in this spreading pathway, viruses are exposed to host anti-virus defense systems. In contrast, direct infection to a neighboring cell is considered to be beneficial for the virus in terms of evasion from the host anti-virus defense. There are two typical manners in infection to "*right next door*": one is the virus transmission through cell-cell fusion by forming syncytium without production of progeny virions, and the other is mediated by virions without virus diffusion, generally designated cell-to-cell transmission [1,2].

The cell-cell fusion infection pathway is characteristic for a variety of virus such as paramyxoviruses, herpesviruses, some retroviruses, and so on. For example in the case of measles virus belonging to *Paramyxoviridae*, infection is initiated by the interaction of the viral hemagglutinin glycoprotein with host cell surface receptors. The virus penetrates into the cell through membrane fusion mediated by the interaction of the fusion glycoprotein. In later stages of infection, newly synthesized glycoproteins accumulate at the cell membrane resulting in fusion of the infected cell with neighboring cells by producing syncytia. Thus, viruses can spread from cell to cell without producing *cell-free* virus particles.

The examples of the cell-to-cell transmission are diverse, and these mechanisms are dependent on pairs of viruses and host cells. Vaccinia virus particles bound on the filopodium of an infected cell are repelled toward neighboring uninfected cells by the formation of filopodia using actin filament [3]. The filopodia direct viruses to uninfected cells. Immunotropic viruses including retroviruses utilize an immunological synapse, designed as virological synapses for the cell-to-cell transmission [4–7]. Claudin-1 and occludin, components of tight junction, are involved in hepatitis C virus (HCV) entry through the cell-to-cell transmission [8,9]. The cell-to-cell transmission through tight junction is also observed in other viruses which infect epithelial layers [10,11]. These retroviruses and HCV remain on the surface of an infected cell even after budding. The uninfected cells adjacent to these infected cells can accept or take over viruses from